LOW-SPEED AND HIGH-SPEED CORRELATION OF SMART ACTIVE FLAP ROTOR LOADS

Sesi Kottapalli
Flight Vehicle Research and Technology Division
NASA Ames Research Center
Moffett Field, California
Sesi.B.Kottapalli@nasa.gov

Measured, open loop and closed loop data from the SMART rotor test in the NASA Ames 40- by 80- Foot Wind Tunnel are compared with CAMRAD II calculations. One open loop high-speed case and four closed loop cases are considered. The closed loop cases include three high-speed cases and one low-speed case. Two of these high-speed cases include a 2 deg flap deflection at 5P case and a test maximum-airspeed case. This study follows a recent, open loop correlation effort that used a simple correction factor for the airfoil pitching moment Mach number. Compared to the earlier effort, the current open loop study considers more fundamental corrections based on advancing blade aerodynamic conditions. The airfoil tables themselves have been studied. Selected modifications to the HH-06 section flap airfoil pitching moment table are implemented. For the closed loop condition, the effect of the flap actuator is modeled by increased flap hinge stiffness. Overall, the open loop correlation is reasonable, thus confirming the basic correctness of the current semi-empirical modifications; the closed loop correlation is also reasonable considering that the current flap model is a first generation model. Detailed correlation results are given in the paper.

Notation

c_m	Pitching moment coefficient
C_T	Helicopter thrust coefficient
KTEF	Flap hinge stiffness, ft-lb/rad
M	Mach number
NP	Integer (N) multiple of rotor speed
Per rev	Per revolution
R*m*Pt*n*	NASA wind tunnel Run "*m*" Point "*n*"
α	Angle of attack
α_s	Rotor shaft angle
μ	Rotor advance ratio
σ	Rotor solidity ratio

Sign Convention

Chordwise moment, + tip toward trailing edge.
Flap deflection, + trailing edge down.
Flap lift, + up; flap chordwise force, + toward leading edge.
Flatwise moment, + tip up.
Pitch link load, + in tension.
Torsion moment, + leading edge up.

Presented at the American Helicopter Society Aeromechanics Specialists' Conference, San Francisco, CA, January 20-22, 2010. *This is a work of the U.S. Government and is not subject to copyright protection in the U.S.*

Introduction

DARPA, Boeing, the U.S. Army, and NASA have recently completed a full-scale wind tunnel test of the Boeing Smart Material Advanced Rotor Technology (SMART) bearingless rotor, Refs. 1-2. The data from this wind tunnel test is being used to validate the Helicopter Quieting Program noise prediction tools as well as to improve the ability to predict rotor performance, vibration, and loads. The SMART rotor is a next generation rotor system that offers high bandwidth on-blade active trailing edge flaps that will provide unique modeling challenges for the vibration and noise prediction tool sets. Reference 3 contains a description of the SMART rotor.

The current analytical work is a follow-on study to the recent, open loop correlation effort reported in Ref. 4. Whereas Ref. 4 addressed a single high-speed operating condition at $\mu = 0.30$, the current study covers both low-speed and high-speed regimes (μ = 0.20, 0.30, and 0.37), and includes both open and closed loop conditions. Note that for the $\mu = 0.30$ condition, two test runs are involved. In Ref. 4, the $\mu = 0.30$ open loop test run had some 1P voltage command signal sent to the flap. The current study considers a different, simpler open loop test run, with no varying voltage command inputs to the flap. For the open loop condition, Table 1, the current study further explores the high-speed

compressibility consideration brought up in Ref. 4, and improves the airfoil tables by introducing modifications to the flap airfoil tables at transonic Mach numbers. This study also considers four closed loop test conditions, Table 1. For the closed loop cases, the effect of the SMART flap's piezoelectric actuator in its active state is modeled by appropriately increasing the analytical flap hinge stiffness (more details on the flap model are given later in this paper). Overall, this paper considers two types of analytical models that involve the flap aerodynamics and separately, the flap stiffness.

The objective of this correlation effort is to establish the best comprehensive analysis model of the SMART rotor to be used as a vibration and loads prediction tool. The short-term program goal is to use the analytical model for pre-flight predictions prior to an anticipated, future flight test of the SMART rotor. The ultimate goal of this effort is to provide the blade designer with reliable predictive tools that can lead to optimized blades, with reductions in the money and time spent on wind tunnel and flight tests.

The basic rotor without the smart material technology is derived from the five-bladed MD 900 Explorer main rotor. It has a radius of 16.9 ft and a nominal 1g thrust of approximately 6,000 lbs, Refs. 5-6. References 6-8 describe the 1992 wind tunnel test conducted at NASA Ames with the MDART rotor, a pre-production version of the Explorer rotor. The blades and flexbeams are made of fiberglass and the pitchcase, for which high stiffness is essential, is made of graphite. The flexbeam extends to approximately 0.20R. The implementation of the smart material active trailing edge flaps is described in Refs. 1 and 3. Each blade consists of 12% thick HH-10 airfoil sections inboard up to 74% radius, and 9.5% thick HH-06 airfoil sections outboard beyond 84% radius. The SMART rotor trailing edge flap extends from approximately 0.75R to 0.92R.

The present study considers the first step in the prediction of the five-bladed SMART rotor loads. The rotor loads include the blade and flap loads, and the pitch link loads. In this study, a fixed, rigid hub is considered, i.e. the fuselage effects are not included. In total, five cases are considered, four high-speed cases and one low-speed case. The effects of the individual trailing edge flaps on the high-speed rotor loads are considered by studying the following two cases: a 2 deg flap deflection at 5P case followed by the corresponding zero flap deflection case. The rotorcraft comprehensive analysis CAMRAD II (Refs. 9-11) is used to model the SMART rotor.

Measured Wind Tunnel Data

References 1 and 2 contain descriptions of the recent SMART Rotor test in the NASA Ames 40- by 80- Foot Wind Tunnel. The wind tunnel data used in the current paper is taken from Ref. 1.

Results

The results in this paper are given in two parts, open loop and closed loop, Table 1. The corresponding wind tunnel run and point numbers are also shown in Table 1.

Analytical model

The CAMRAD II analytical model used in the current correlation study is briefly described. The SMART rotor blade and flexbeam are modeled using elastic beam elements, with each element having two elastic flap bending, two elastic lag bending, and two torsion degrees of freedom. The blade consists of four beam elements, the torque tube one element, and the flexbeam three elastic elements (plus a rigid element at each end of the flexbeam). The trailing edge flap was modeled as a rigid body, using the measured flap hinge stiffness, flap hinge damping, and flap mass. The flap extends from 0.74R to 0.92R. The aerodynamic model used 20 spanwise panels for the entire blade, 10 inboard of the flap, 6 on the flap (from 0.74R to 0.92R), and 4 outboard of the flap.

Flap model. The trailing edge flap was modeled as a rigid body, using the measured flap hinge stiffness KTEF, flap hinge damping, and flap mass. The actual flap tested in the wind tunnel is mounted to the blade using five equally spaced hinges to minimize stresses. In the current study, the rigid flap is modeled as having one attachment point, at the flap mid-span, through which the flap loads are transmitted to the blade in a concentrated manner. Also, the current simulation is an open loop simulation in which the flap is free to respond dynamically (with prescribed spring stiffness, damping, mass, and inertia) to the aerodynamic environment, and the commanded flap deflection works through the flap spring. The actual flap deflection includes its dynamic response. During the wind tunnel test, for those runs in which the closed loop controller, Ref. 2, was activated, a piezoelectric actuator provided an additional, time-varying actuation to maintain a prescribed flap deflection pattern around the azimuth. In this study, the ability of the closed loop piezoelectric actuator to maintain a prescribed flap deflection is simulated by increasing the flap hinge stiffness KTEF. Earlier, Ref. 4 had considered 1.5X and 2.0X increases in KTEF, but in that open loop effort the emphasis was on matching the blade mid-span torsion moment whereas in the current

closed loop effort, the objective is to match the prescribed flap deflection. In the current open loop case, the baseline value of KTEF is used. The current analytical flap model is a first generation model.

At high-speed, the rolled-up wake model, with single tip vortex and single circulation peak, that was used in Ref. 4 is used. At low-speed, the multiple trailer wake model with consolidation, compression form, that was used in Ref. 12, at $\mu = 0.11$, is also used at the current $\mu = 0.20$.

The overall, stepwise procedure to get a converged, trimmed CAMRAD II run for the SMART rotor is outlined as follows: first, the advance ratio is increased from the hover condition to its final value; and second, for the case with 2 deg flap deflection at 5P, the flap deflection is incrementally increased from 0 deg to the final 2 deg. A small amount of structural damping is introduced to ensure convergence.

The predicted hover torsion frequency, including flap mass and inertia, is 5.8P, and was obtained with a pitch link stiffness of 114,000 lb/ft. During the wind tunnel test, the measured torsion frequency was 5.85P, Ref. 1. Since the above analytical and experimental hover torsion frequencies are sufficiently close to each other, the pitch link stiffness was kept unchanged at its current value throughout this study. Figure 1 shows the frequency fan plot for the SMART rotor, Ref. 1. Table 2 shows the current CAMRAD II calculated SMART rotor blade frequencies.

In the following figures, the open loop results are labeled as "Predicted, HH-06 flap c_m modified", and this refers to the current, compressibility-related, high-speed modifications to the flap pitching moment airfoil table for the outboard HH-06 section, discussed later in more depth. The HH-06 flap c_m has been modified for selected transonic Mach numbers. Also, most of the closed loop results are labeled as "Predicted, 3X KTEF", and this refers to a three-times increase from the baseline flap hinge stiffness.

Open loop, high-speed, $\mu = 0.30$

This operating condition (with a different test run) was considered in Ref. 4 in which a simple Mach number correction factor was applied to the pitching moment. Without getting into CFD-based loads calculations, these compressibility effects are further explored in the current study by modifications to the flap airfoil properties. Several modifications have been tried. For example, in one attempt, the HH-06 section flap lift, drag, and pitching moment were made constant for $M \geq 0.6$, i.e., the flap airfoil properties for $M > 0.6$ were kept the same as for $M = 0.6$. The final modifications and the resulting correlation are described as follows (the flap hinge stiffness KTEF was kept at its baseline value).

Blade loads and pitch link load. Figure 2a shows the current correlation for the blade torsion moment at 0.64R. Both the uncorrected and corrected predictions are shown, with the corrected prediction labeled as "Predicted, HH-06 flap c_m modified". The c_m modifications are described as follows. To improve the advancing blade dip correlation, the flap airfoil pitching moment table for the HH-06 section was modified only for high Mach numbers and negative angles of attack. Also, for the above operating condition the predicted, advancing blade elastic flap deflection is positive, thus further narrowing the extent of the required modifications. To summarize, first, only the HH-06 flap airfoil tables have been modified, and second, these modifications cover high Mach numbers, negative angles of attack, and positive flap deflection (the blade HH-06 airfoil tables have not been modified). Several modifications were studied, and current results show that to get the best correlation, the flap c_m variations for angles of attack $\alpha < -1$ deg need modification. The flap airfoil tables include three flap deflection states only, -4 deg, 0 deg, and +4 deg. In the current study, for $M \geq 0.6$ and flap deflection = +4 deg, the flap c_m was made the same for all $\alpha < -1$ deg (e.g., the flap c_m at $\alpha = -2$ deg is the same as at -1 deg). Figures 2a-2b show the resulting torsion moment correlation at 0.64R and 0.81R. The corresponding flatwise and chordwise bending moment correlations are shown in Figs. 2c-2f, at 0.59R and 0.81R, respectively. The pitch link load correlation is shown in Fig. 2g, and the corresponding half peak-to-peak values are as follows: test, 75 lb and analysis, 77 lb. Figure 2h shows the measured flap deflections (obtained by a Hall effect sensor). Figure 2i compares the measured and predicted time-histories for flap 1. Overall, Figs. 2a-2g show that the correlation is fair at this open loop high-speed condition.

Predicted flap loads. The predicted results have been studied to understand how the trailing edge flap affects the blade behavior, Figs. 2j-2k. Figures 2j-2k show the predicted flap lift and chordwise force acting on the blade. Both uncorrected and corrected loads are shown in Figs. 2j-2k. Clearly, the current compressibility correction reduces the advancing blade flap lift, because of the dynamic response of the flap to the hinge moment, Fig. 2j, thus reducing the nose down torsion moment, Fig. 2a. Figure 2l is a two-vertical-axes azimuthal plot that shows the flap lift, right axis, and the blade torsion moments at 0.64R and 0.81R, left axis. Figure 2l compares the azimuthal variations of the flap lift acting on the blade and the blade torsion moment, and these two have opposite phase. Since the blade

quarter chord is forward of the flap quarter chord (by roughly 0.5 blade chord lengths), an upward flap force introduces a nose down twisting moment on the blade.

Closed loop

For the closed loop condition, a parametric study has been conducted varying the flap hinge stiffness KTEF with the primary objective of matching the test flap deflection time history for the commanded 2 deg flap at 5P case, discussed below under Case 1. However, another basic variation, the blade mid-span torsion moment time history for the 0 deg flap case, Case 2, was also considered for qualitative agreement. It has been found that the best trade-off between matching the 2 deg amplitude flap deflection time history in Case 1 and at the same time, qualitatively correlating the blade mid-span torsion moment in Case 2, is possible with a 3X baseline KTEF, shown later in Fig. 3b (Case 1) and Fig. 4c (Case 2), respectively.

Case 1. High-speed, μ = 0.30, 2 deg flap at 5P (90 deg phase). Figure 3a shows the measured flap deflections for all five blades. For flap 1, Fig. 3b shows the measured time history and the effect of varying the flap hinge stiffness KTEF. Figure 3b shows that the best KTEF is 3X its baseline value. Increasing KTEF to, for example, 3.5X its baseline value may not help, as this will further reduce the retreating side amplitude, already < 2 deg. This may be a consequence of the current azimuthally non-varying KTEF.

Figures 3c-3d show the torsion moment correlation at 0.64R and 0.81R. The corresponding flatwise and chordwise bending moment correlations are shown in Figs. 3e-3h, at 0.59R and 0.81R, respectively. The pitch link load correlation is shown in Fig. 3i, and the corresponding half peak-to-peak values are as follows: test, 147 lb and analysis, 154 lb. Overall, Figs. 3b-3i show that the correlation is fair for torsion, poor for bending, with overprediction on the advancing side.

Figures 3j-3k show the predicted flap forces acting on the blade and the effect of the flap lift on the blade torsion moment. The conclusions from Figs. 3j-3k are the same as those for the open loop case.

Case 2. High-speed, μ = 0.30. Figure 4a shows the measured flap deflections for this 0 deg flap case. Figure 4b shows the measured and predicted flap deflections for flap 1. Figure 4c shows the torsion moment correlation at 0.64R. From Fig. 4c it can be seen that a 3X KTEF qualitatively preserves the important advancing blade dip. Figure 4d shows the torsion moment correlation at 0.81R. The corresponding flatwise and chordwise bending moment correlations are shown in Figs. 4e-4h, at 0.59R and 0.81R, respectively. The pitch link load correlation is shown in Fig. 4i, and the corresponding half peak-to-peak values are as follows: test, 56 lb and analysis, 51 lb. Overall, Figs. 4c-4h show that the correlation is fair at this high-speed condition.

Figures 4j-4k show the predicted flap forces acting on the blade and the effect of the flap lift on the blade torsion moment. The conclusions from Figs. 4j-4k are the same as those for the open loop case.

Case 3. High-speed, μ = 0.37, test maximum airspeed. Figure 5a shows the measured and predicted flap deflections for flap 1 for this 0 deg flap case (the other four test flaps had similar amplitudes and their measured time histories are not shown). Figures 5b-5c show the torsion moment correlation at 0.64R and 081R, respectively. The torsion moment waveform does not undergo any qualitative change when μ is increased from 0.30 to 0.37, the test maximum airspeed (Figs. 4c and 5b). The corresponding flatwise and chordwise bending moment correlations are shown in Figs. 5d-5g, at 0.59R and 0.81R, respectively. The pitch link load correlation is shown in Fig. 5h, and the corresponding half peak-to-peak values are as follows: test, 111 lb and analysis, 60 lb. Overall, Figs. 5a-5h show that the correlation is fair at this high-speed condition, with underprediction in the pitch link load.

Figures 5i-5j show the predicted flap forces acting on the blade and the effect of the flap lift on the blade torsion moment. The conclusions from Figs. 5i-5j are the same as those for the open loop case.

Case 4. Low-speed, μ = 0.20. Figure 6a shows the measured and predicted flap deflections for flap 1 for this 0 deg flap case (the other four test flaps had similar amplitudes and their measured time histories are not shown). Figures 6b-6c show the torsion moment correlation at 0.64R and 081R, respectively. The corresponding flatwise and chordwise bending moment correlations are shown in Figs. 6d-6g, at 0.59R and 0.81R, respectively. The pitch link load correlation is shown in Fig. 6h, and the corresponding half peak-to-peak values are as follows: test, 40 lb and analysis, 38 lb. Overall, Figs. 5a-5h show that the correlation is fair at this low-speed condition.

Figures 6i-6j show the predicted flap forces acting on the blade and the effect of the flap lift on the blade torsion moment. The conclusions from Figs. 6i-6j are the same as those for the open loop case.

X-Y correlation for all cases, open and closed loop

Figures 7a-7d show the measured and calculated data in x-y format for the torsion, flatwise, and chordwise moments, and the pitch link load, respectively, for all cases, both open and closed loop. Figure 7a shows that the torsion moment correlation is fair, but could be improved. Figure 7b shows that the flatwise moment correlation is also fair. Figure 7c shows that the chordwise moment is underpredicted. Figure 7d shows that the pitch link load correlation is fair, with some underprediction.

Use of Multi-Element Airfoil Code MSES

A compressibility-related correction based on modified airfoil tables has been used for the open loop correlation. With the open loop results as background, a separate follow-on study has been initiated to get improved airfoil tables without resorting to the semi-empirical modifications like the current modifications. The two-dimensional, multi-element airfoil code MSES will be used to systematically generate new airfoil tables. A brief description of MSES, Refs. 13-14, follows.

MSES can analyze single and multi-element airfoils at transonic Mach numbers. The boundary layer transition can be either forced or predicted. A finite volume discretization of the steady Euler equations with an intrinsic streamline grid is used. The boundary layers and trailing wakes are described by a two-equation integral model. The inviscid and viscous regions are fully coupled using the boundary layer displacement thickness. Newton's method is used to solve the overall system.

Preliminary, first-pass MSES results have been obtained for the HH-06 airfoil only (no flap) at M = 0.6. Based on the sensitivity to the airfoil geometry as shown by these results, it has been concluded that accurate airfoil and flap geometries are needed. That is, the geometry of the actual SMART rotor that was tested in the wind tunnel is needed, and this includes both the HH-06 and HH-10 airfoils, with and without the SMART flap. These geometries are being obtained currently.

Conclusions

The prediction of SMART active trailing edge flap rotor loads was considered in this analytical study for both open loop and closed loop conditions. The following five cases were considered: 1) Open loop, high-speed, $\mu = 0.30$; 2) closed loop, high-speed, $\mu = 0.30$, with 2 deg trailing edge flap deflection at 5P; 3) closed loop, high-speed, $\mu = 0.30$; 4) closed loop, high-speed, $\mu = 0.37$, the test maximum-airspeed; and 5) closed loop, low-speed, $\mu = 0.20$. Measured data from the NASA Ames 40- by 80- Foot Wind Tunnel were compared with CAMRAD II predictions.

This study followed a recent, open loop correlation effort that used a simple correction factor for the airfoil pitching moment Mach number. For the open loop condition, the current study considered more fundamental corrections based on advancing blade aerodynamic conditions. The airfoil tables themselves were studied, and selected modifications to the HH-06 flap airfoil pitching moment table were implemented. For the closed loop conditions, the effect of the SMART flap actuator was modeled by increased flap hinge stiffness.

For the open loop case, the correlation was reasonable, thus confirming the basic correctness of the current semi-empirical modifications. Since only the HH-06 section flap c_m was modified (for selected Mach numbers, blade angles of attack, and flap deflection), this study addressed only a limited portion of the SMART rotor airfoil table database. The new goal is to get improved airfoil tables without resorting to empiricisms, based completely on transonic airfoil aerodynamics. To this end, a follow-on study that uses the two-dimensional, transonic, multi-element airfoil code MSES has been initiated.

For the closed loop cases, the correlation was reasonable considering the relatively simple, first generation flap model that was used.

Specific conclusions from the current study follow.

1. At low-speed, the correlation was fair.
2. At high-speed, the conclusions are as follows:
   a. For zero flap deflection, the correlation was fair, but could be improved. At the test maximum-airspeed, the correlation was fair, except for the chordwise bending as noted below.
   b. For the 5P, 2 deg flap case, the effect of the flap motion was reasonably captured. The correlation was fair for torsion, poor for bending, with overprediction on the advancing side.
   c. The pitch link load correlation was fair, with some underprediction.
   d. Generally, the chordwise bending moments were underpredicted.

e. The blade torsion moment depends on the flap lift acting on the blade, and it was found that the current compressibility-related modifications reduce the predicted flap lift, resulting in improved correlation.

References

1. Straub, F. K., Anand, V. R., Birchette, T. S., and Lau, B. H., "Wind Tunnel Test of the SMART Active Flap Rotor," American Helicopter Society 65th Annual Forum Proceedings, Grapevine, TX, May 27-29, 2009.

2. Hall, S. R., Anand, V. R., Straub, F. K., and Lau, B.H., "Active Flap Control of the SMART Rotor for Vibration Reduction," American Helicopter Society 65th Annual Forum Proceedings, Grapevine, TX, May 27-29, 2009.

3. Straub, F. K. and Anand, V.R., "Whirl Tower Test and Analysis of the SMART Material Actuated Rotor Technology (SMART) Active Flap Rotor," American Helicopter Society 63rd Annual Forum Proceedings, Virginia Beach, VA, May 1-3, 2007.

4. Kottapalli, S., and Straub, F.K., "Correlation of SMART Active Flap Rotor Loads," American Helicopter Society 65th Annual Forum Proceedings, Grapevine, TX, May 27-29, 2009.

5. Murrill, R.J., Hamilton, B.K., Anand, V.R., Lauzon, D.M., and Tuttles, B., "Bearingless Main Rotor Whirl Test: Design, Analysis, and Test Results," American Helicopter Society 49th Annual Forum Proceedings, St. Louis, MO, May 19-21, 1993.

6. McNulty, M., Jacklin, S., and Lau, B., "A Full-Scale Test of the McDonnell Douglas Advanced Bearingless Rotor in the NASA Ames 40- by 80- Foot Wind Tunnel," American Helicopter Society 49th Annual Forum Proceedings, St. Louis, MO, May 19-21, 1993.

7. Khanh, K., McNulty, M., Anand, V., and Lauzon, D., "Aeroelastic Stability of the McDonnell Douglas Advanced Bearingless Rotor" American Helicopter Society 49th Annual Forum Proceedings, St. Louis, MO, May 19-21, 1993.

8. Jacklin, S. J., Lau, B. H., Nguyen, K. Q., Smith, R. L., and McNulty, M.J., "Full-Scale Wind Tunnel Test of the McDonnell Douglas Five-Bladed Advanced Bearingless Rotor: Performance, Stability, Loads, Control Power, Vibration and HHC Data," American Helicopter Society, American Helicopter Society Aeromechanics Specialists Conference, San Francisco, CA, January 19-21, 1994.

9. Johnson, W. "CAMRAD II, Comprehensive Analytical Model of Rotorcraft Aerodynamics and Dynamics," Johnson Aeronautics, Palo Alto, California, 1992-1999.

10. Johnson, W., "Technology Drivers in the Development of CAMRAD II," American Helicopter Society, American Helicopter Society Aeromechanics Specialists Conference, San Francisco, CA, January 19-21, 1994.

11. Johnson, W., "A General Free Wake Geometry Calculation for Wings and Rotors," American Helicopter Society 51st Annual Forum Proceedings, Ft. Worth, TX, May 9-11, 1995.

12. Kottapalli, S., "Calculation of Hub Loads at Low Airspeeds with Active Control," American Helicopter Society 63rd Annual Forum Proceedings, Virginia Beach, VA, May 1-3, 2007.

13. Drela. M. and Giles. M.B., "Viscous-Inviscid Analysis of Transonic and Low Reynolds Number Airfoils," *AIAA Journal*, Vol. 25, (10), October 1987, pp. 1347-1355.

14. Drela, M., "Newton Solution of Coupled Viscous/Inviscid Multielement Airfoil Flows," AIAA 21st Fluid Dynamics, Plasma Dynamics and Lasers Conference, June 18-20, 1990, Seattle, WA, AIAA-90-1470.

Table 1. SMART rotor open and closed loop correlation cases.

Correlation Cases	Run, Point	C_T/σ	α_s	μ
Open. High-speed, 123 knots	57, 33	0.074	-9.1^0	0.30
Closed, Case 1. High-speed, 123 knots, 2^0 at 5P flap	46, 92	0.080	-9.1^0	0.30
Closed, Case 2. High-speed, 123 knots	46, 94	0.080	-9.1^0	0.30
Closed, Case 3. High-speed, 155 knots, test max-airspeed	63, 56	0.065	-9.3^0	0.37
Closed, Case 4. Low-speed, 83 knots	49, 107	0.075	$+2.0^0$	0.20

Table 2. Predicted SMART rotor blade frequencies, 100% NR.

Blade Mode	Frequency (per rev)
Chord 1	0.564
Flap 1	1.037
Flap 2	2.816
Chord 2	4.409
Flap 3	4.537
Torsion 1	5.797

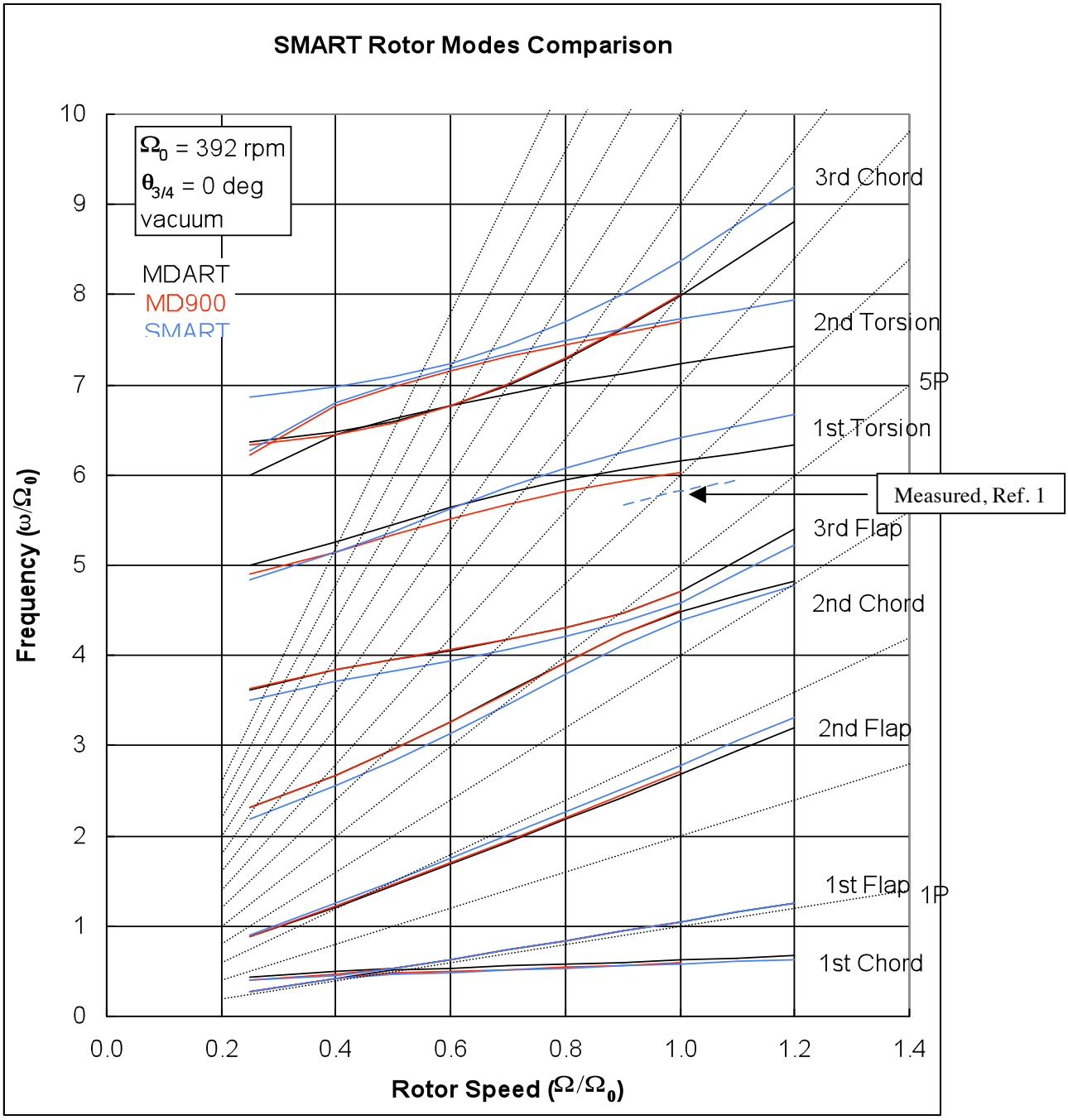

Fig. 1. SMART rotor fan plot, Ref. 1.

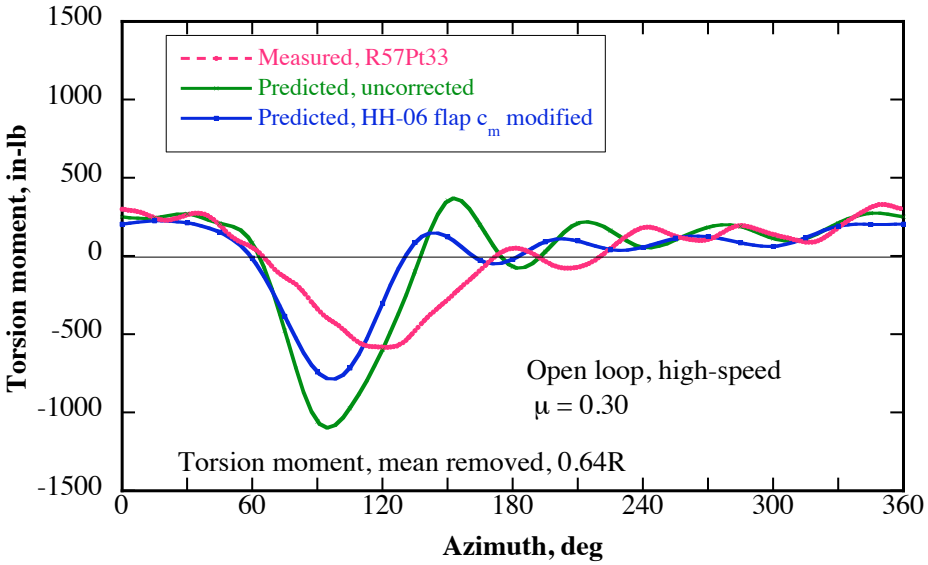

Fig. 2a. Torsion moment correlation, 0.64R, open loop.

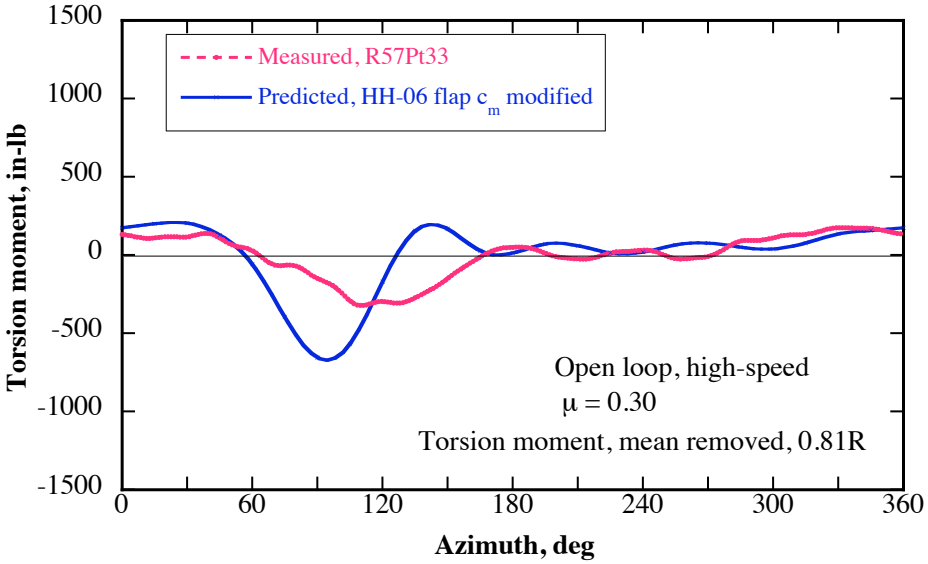

Fig. 2b. Torsion moment correlation, 0.81R, open loop.

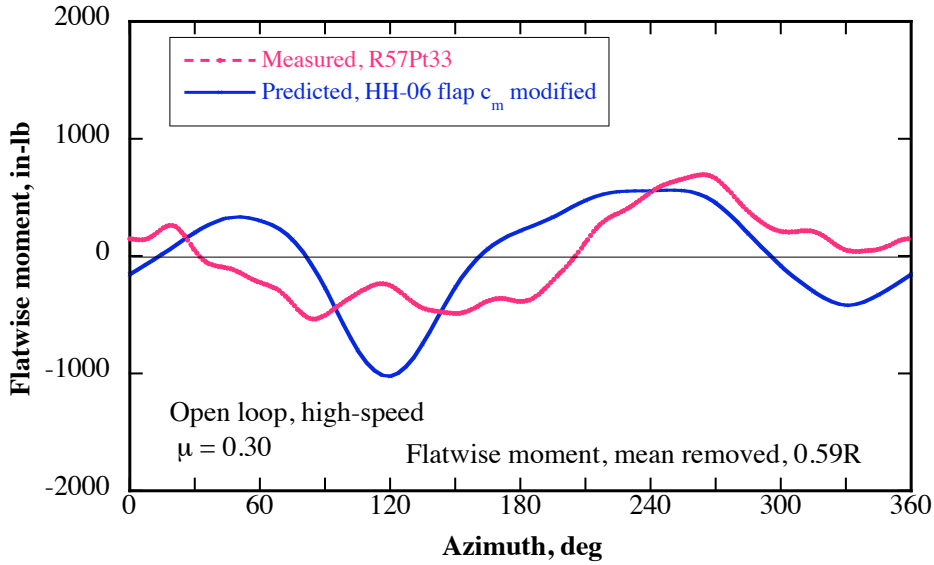

Fig. 2c. Flatwise bending moment correlation, 0.59R, open loop.

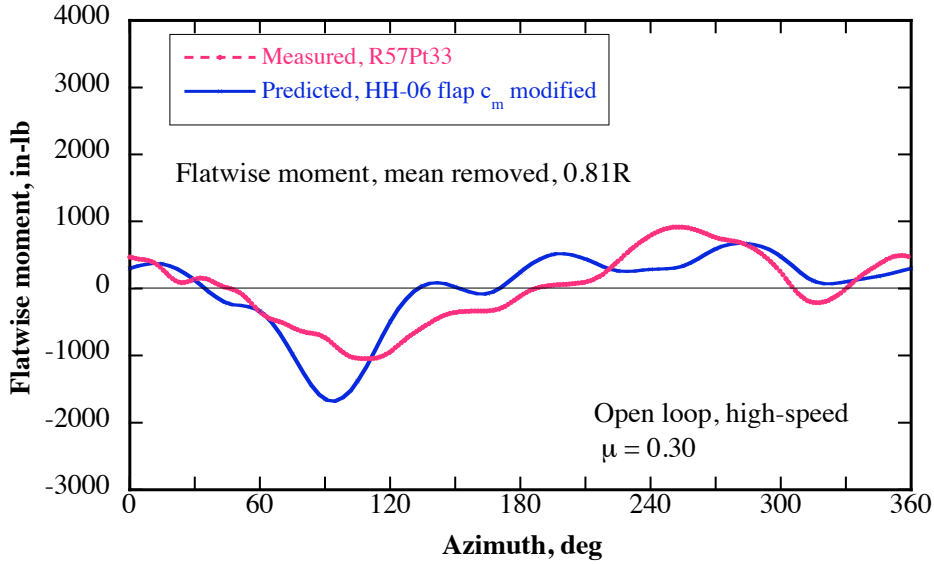

Fig. 2d. Flatwise bending moment correlation, 0.81R, open loop.

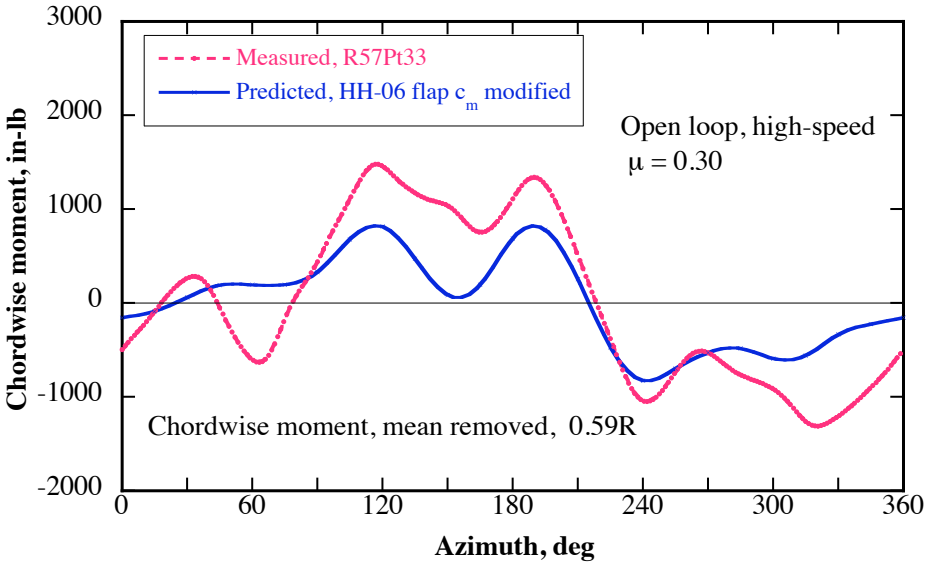

Fig. 2e. Chordwise bending moment correlation, 0.59R, open loop.

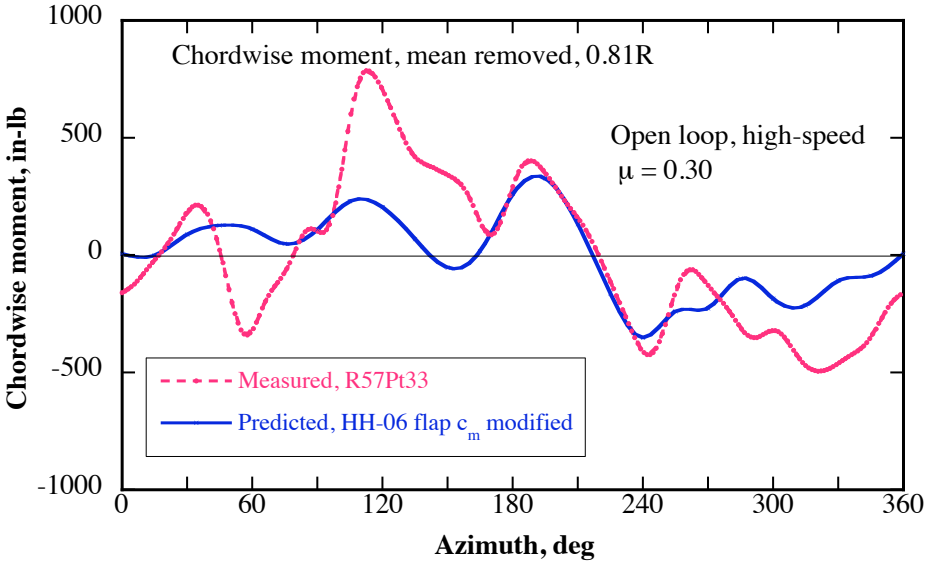

Fig. 2f. Chordwise bending moment correlation, 0.81R, open loop.

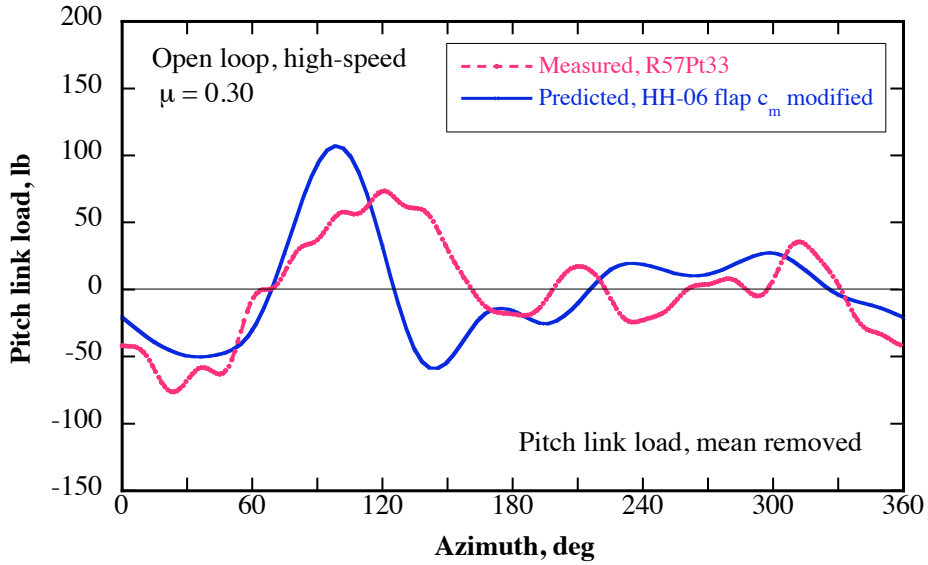

Fig. 2g. Pitch link load correlation, open loop.

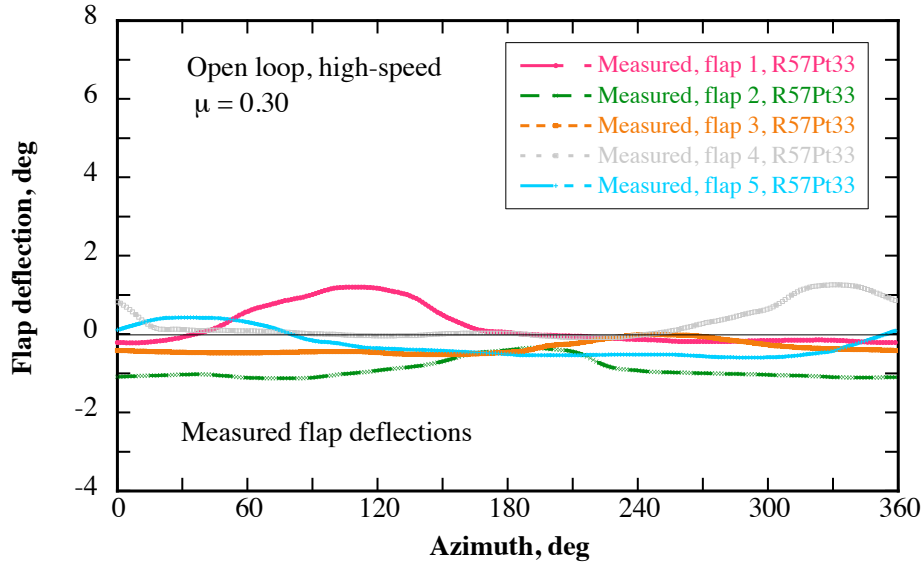

Fig. 2h. Measured flap deflections, open loop.

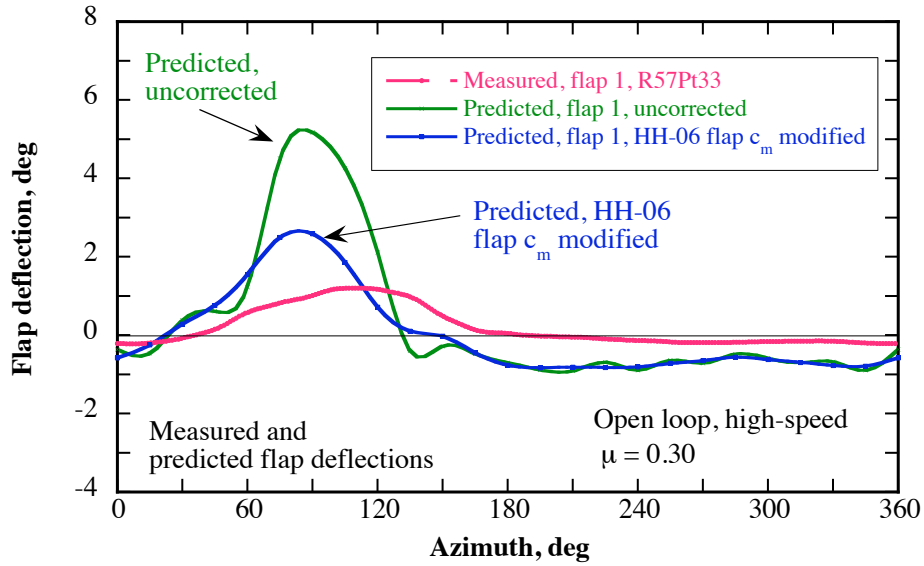

Fig. 2i. Predicted and measured flap deflections, open loop.

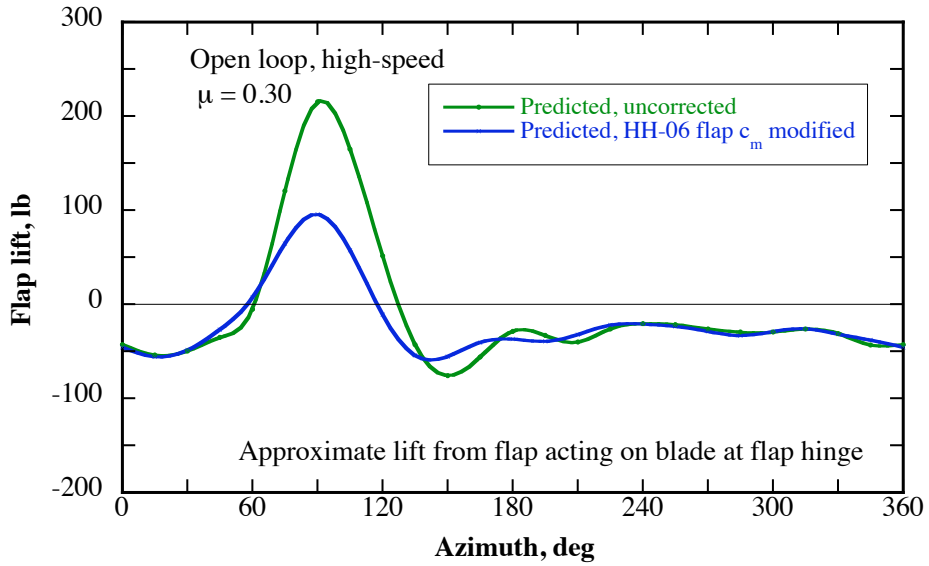

Fig. 2j. Predicted lift force, open loop.

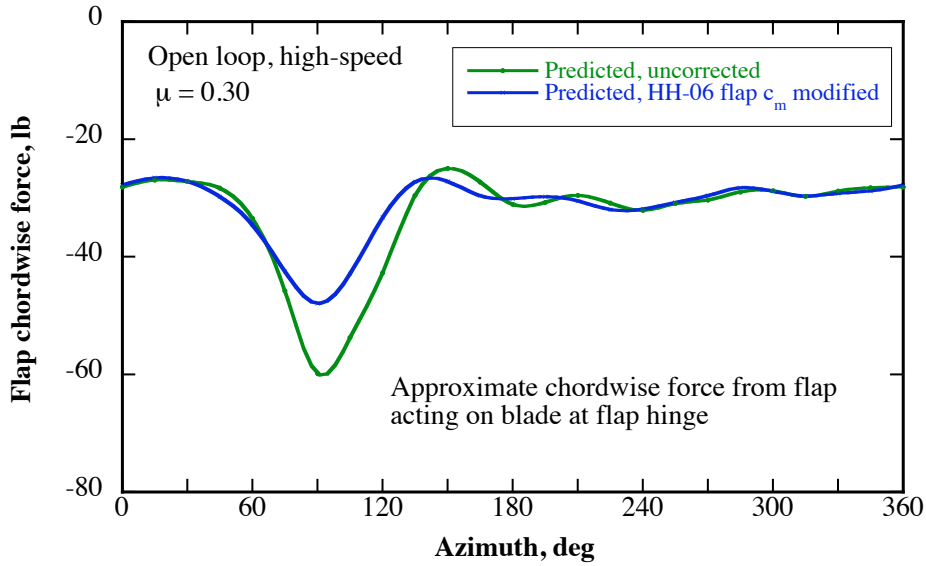

Fig. 2k. Predicted chordwise force, open loop.

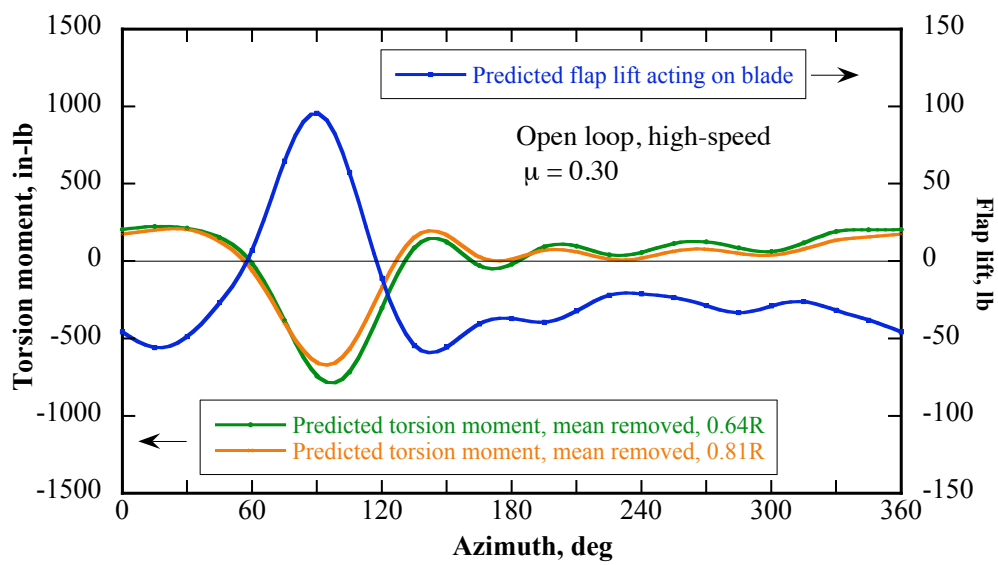

Fig. 2l. Predicted effect of flap, open loop.

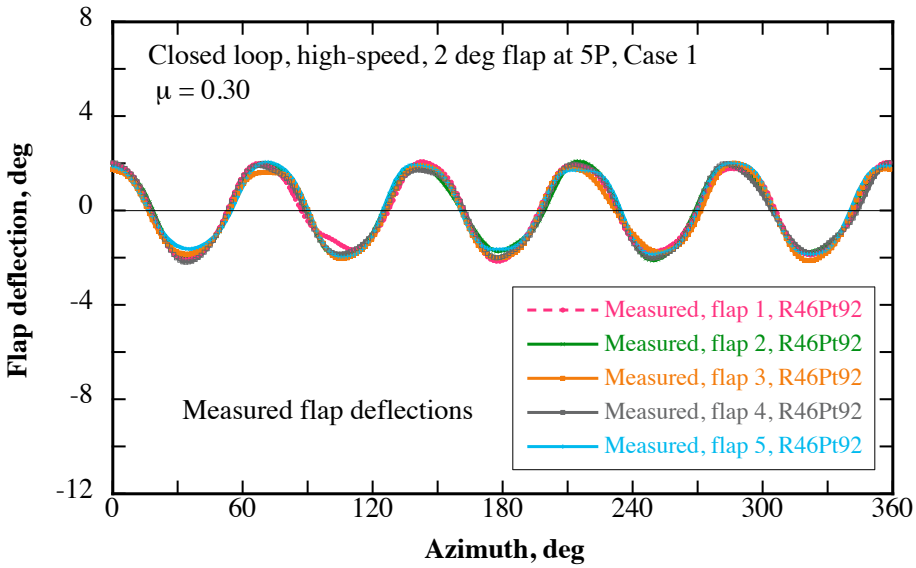

Fig. 3a. Measured flap deflections, closed loop Case 1.

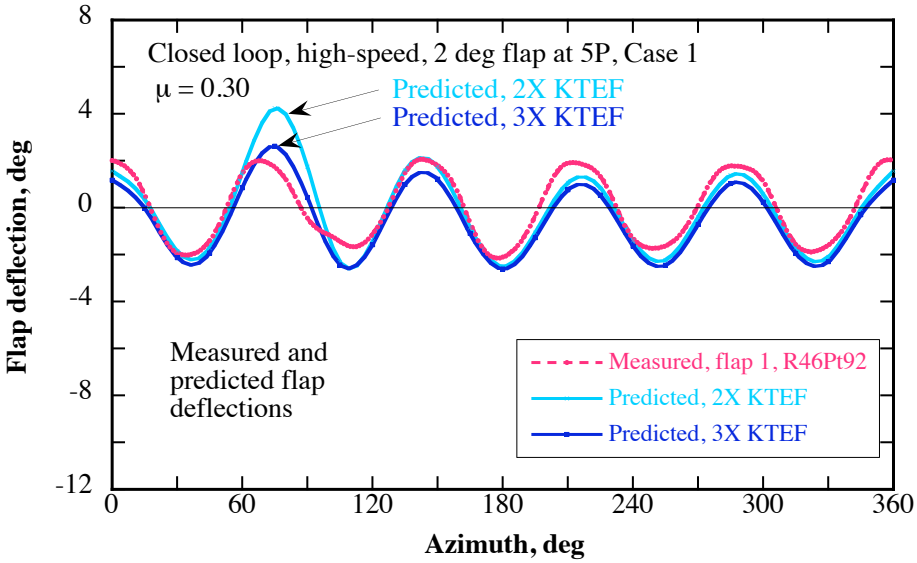

Fig. 3b. Measured and predicted flap deflections, closed loop Case 1.

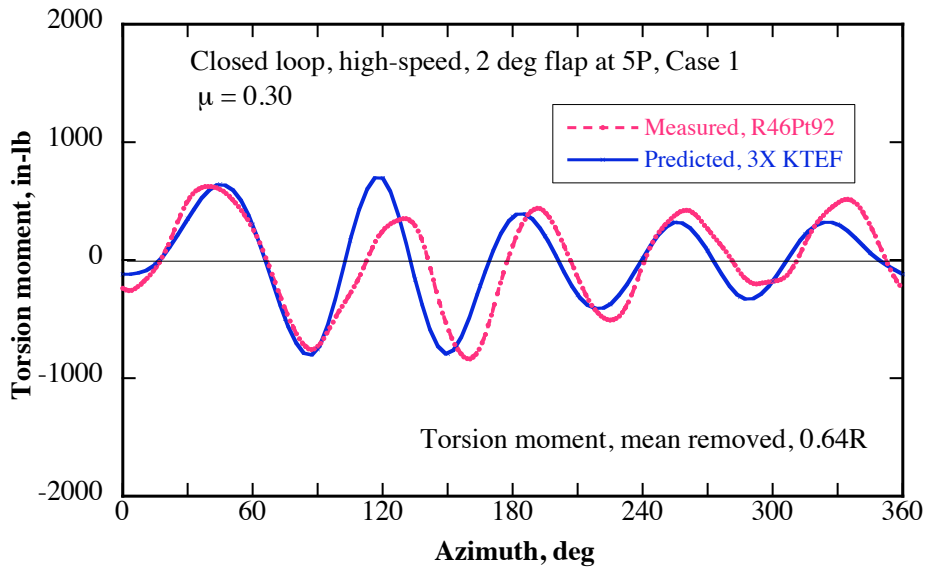

Fig. 3c. Torsion moment correlation, 0.64R, closed loop Case 1.

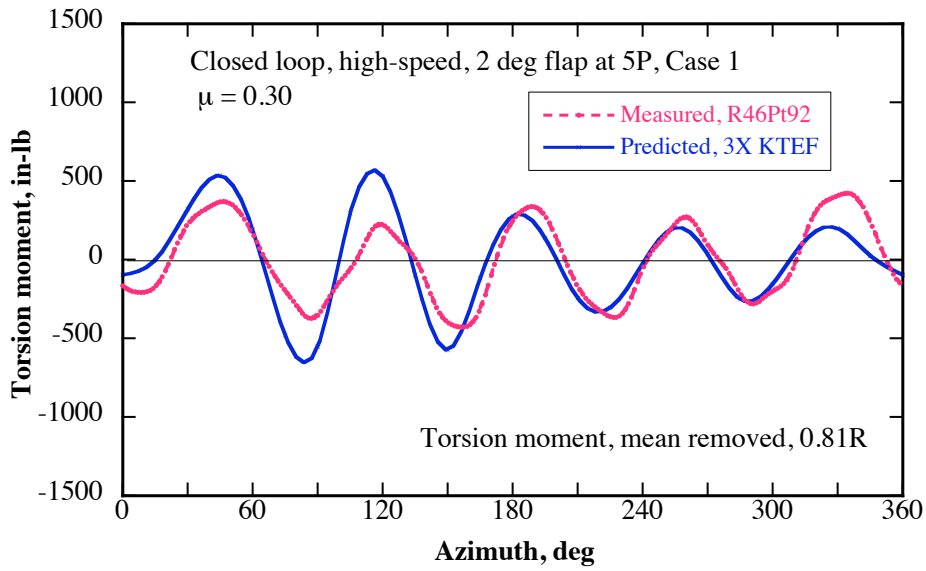

Fig. 3d. Torsion moment correlation, 0.81R, closed loop Case 1.

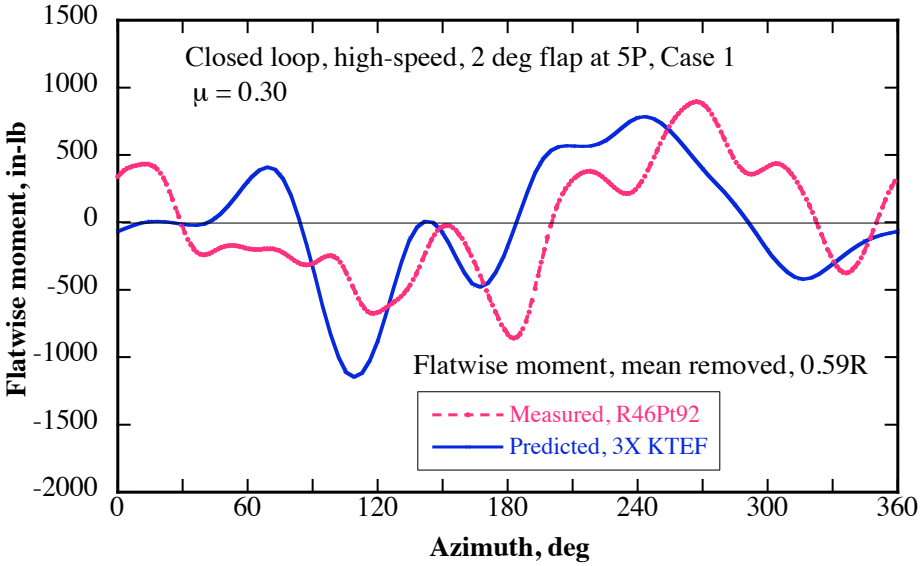

Fig. 3e. Flatwise moment correlation, 0.59R, closed loop Case 1.

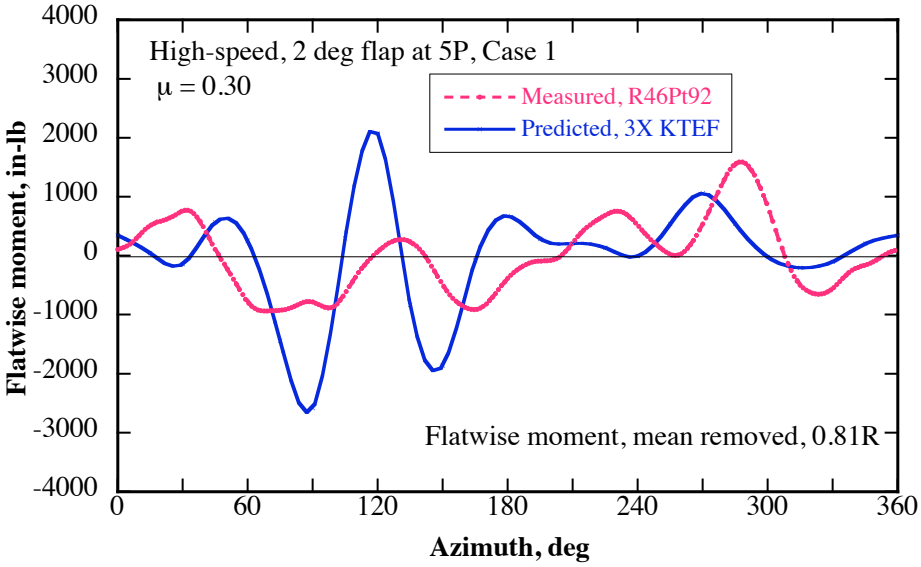

Fig. 3f. Flatwise moment correlation, 0.81R, closed loop Case 1.

.

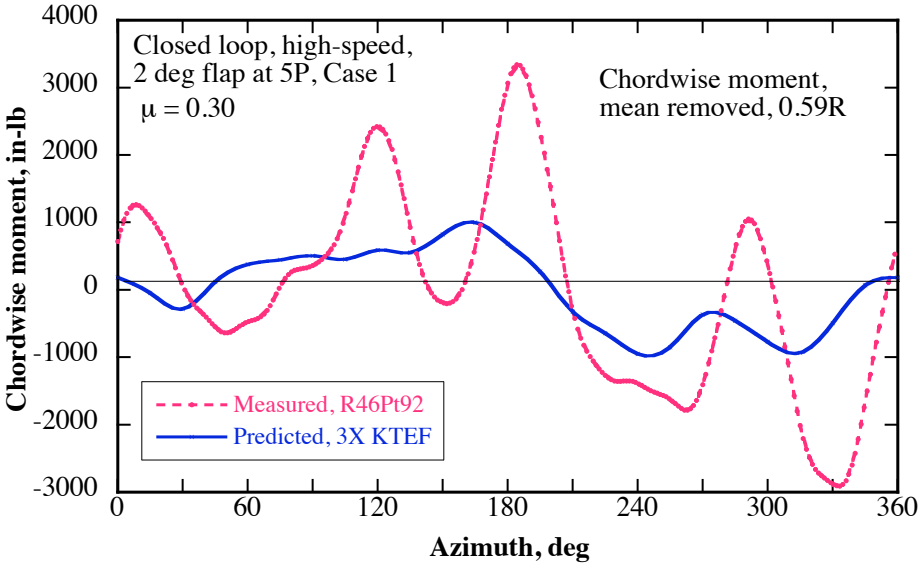

Fig. 3g. Chordwise moment correlation, 0.59R, closed loop Case 1.

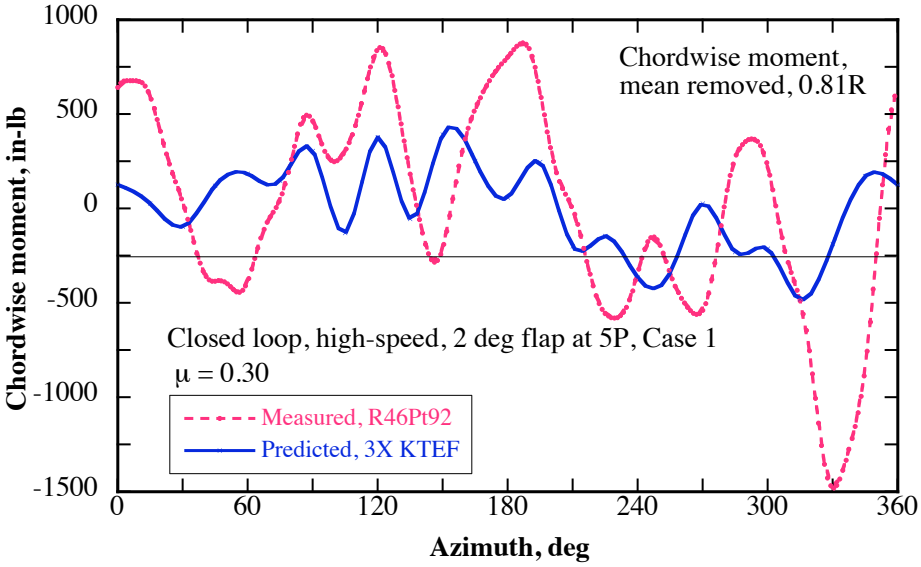

Fig. 3h. Chordwise moment correlation, 0.81R, closed loop Case 1.

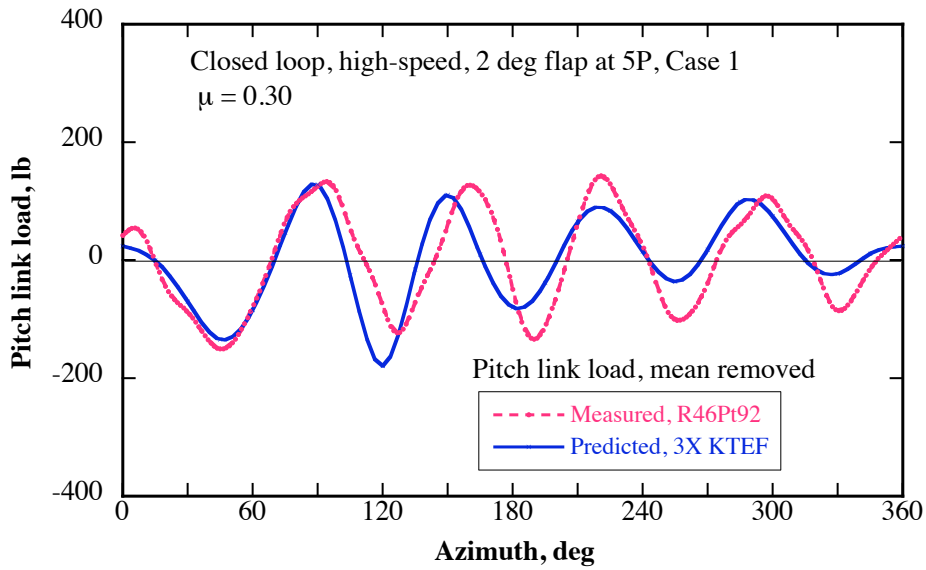

Fig. 3i. Pitch link load correlation, closed loop Case 1.

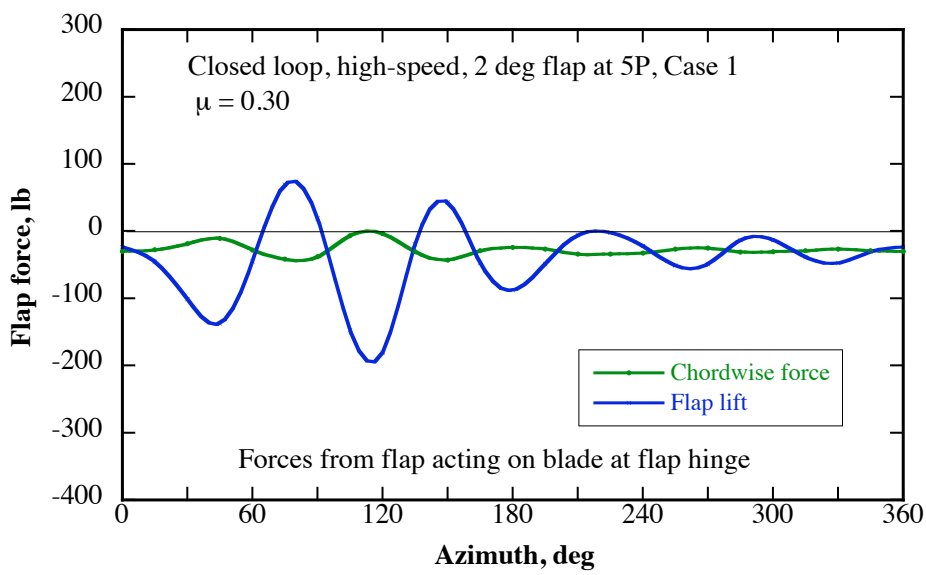

Fig. 3j. Predicted flap forces, closed loop Case 1.

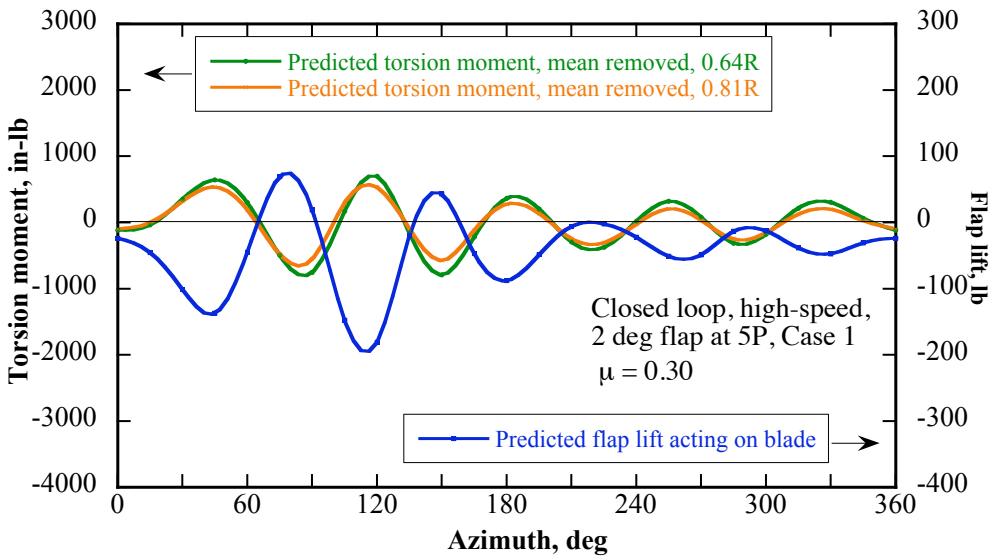

Fig. 3k. Predicted effect of flap on blade, closed loop Case 1.

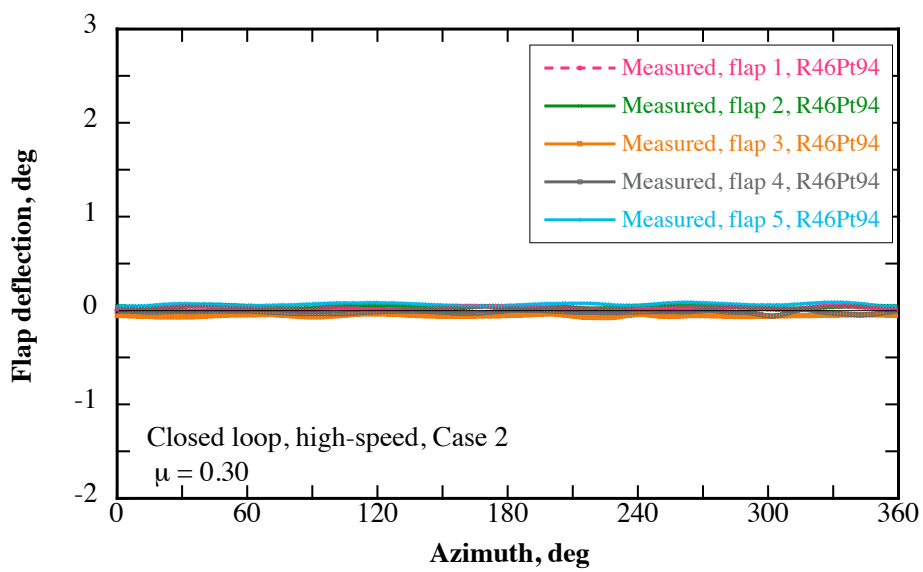

Fig. 4a. Measured flap deflections, closed loop Case 2.

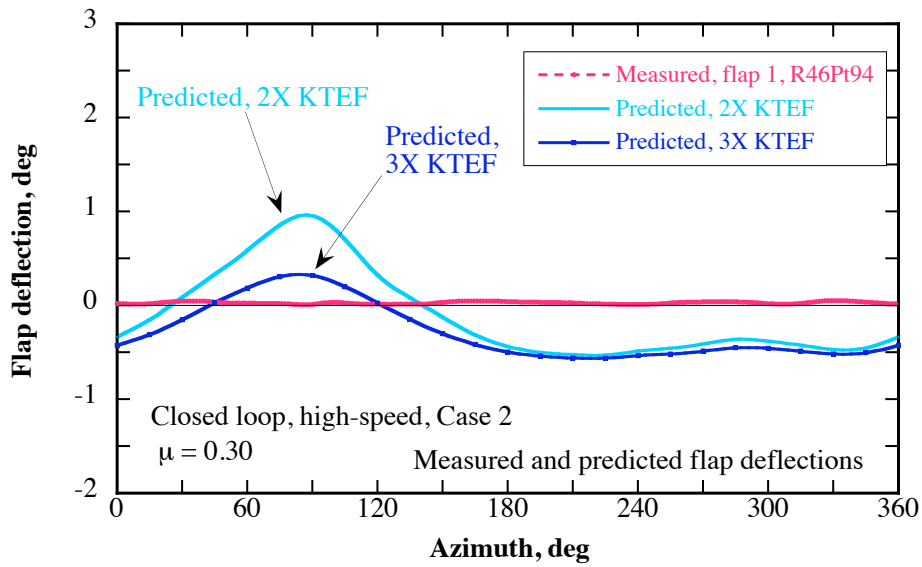

Fig. 4b Measured and predicted flap deflections, closed loop Case 2.

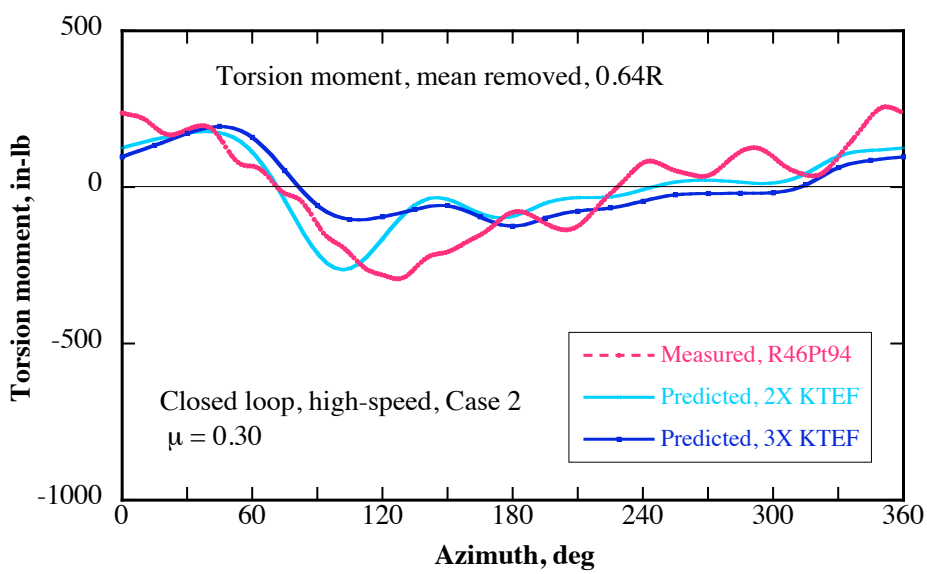

Fig. 4c. Torsion moment correlation, 0.64R, closed loop Case 2.

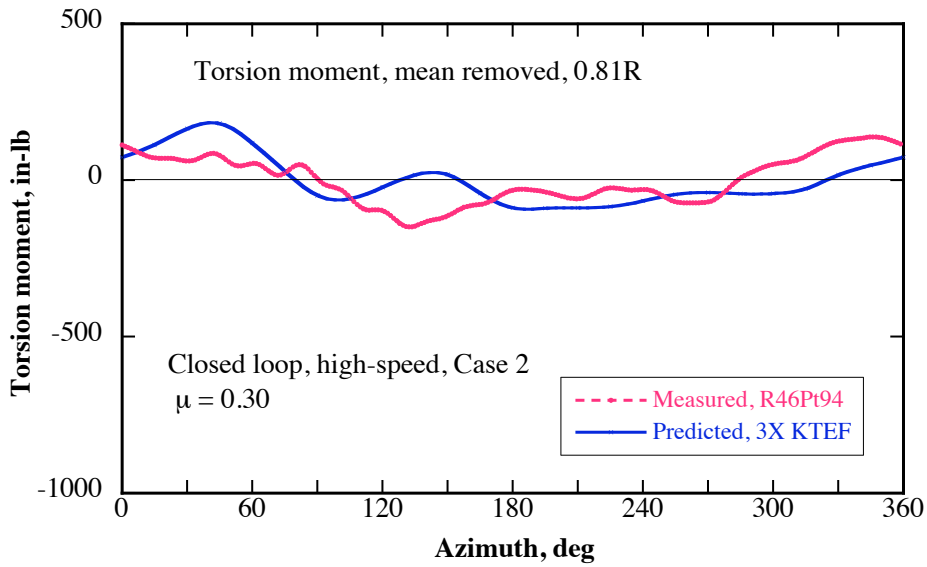

Fig. 4d. Torsion moment correlation, 0.81R, closed loop Case 2.

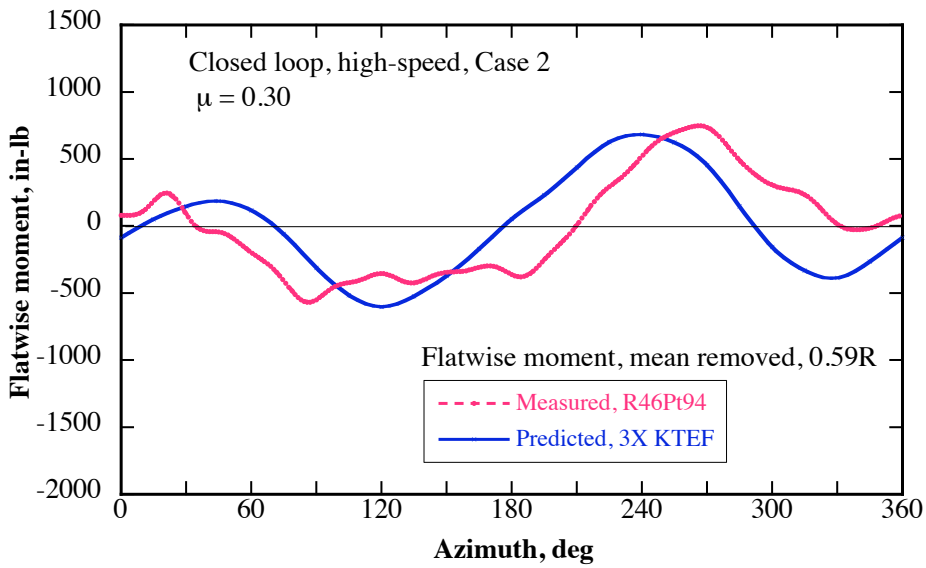

Fig. 4e. Flatwise moment correlation, 0.59R, closed loop Case 2.

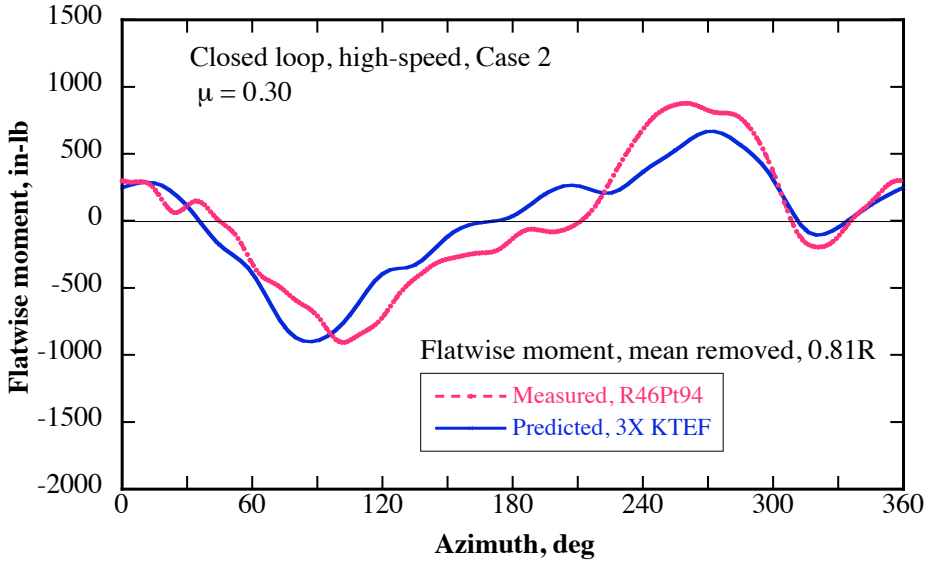

Fig. 4f. Flatwise moment correlation, 0.81R, closed loop Case 2.

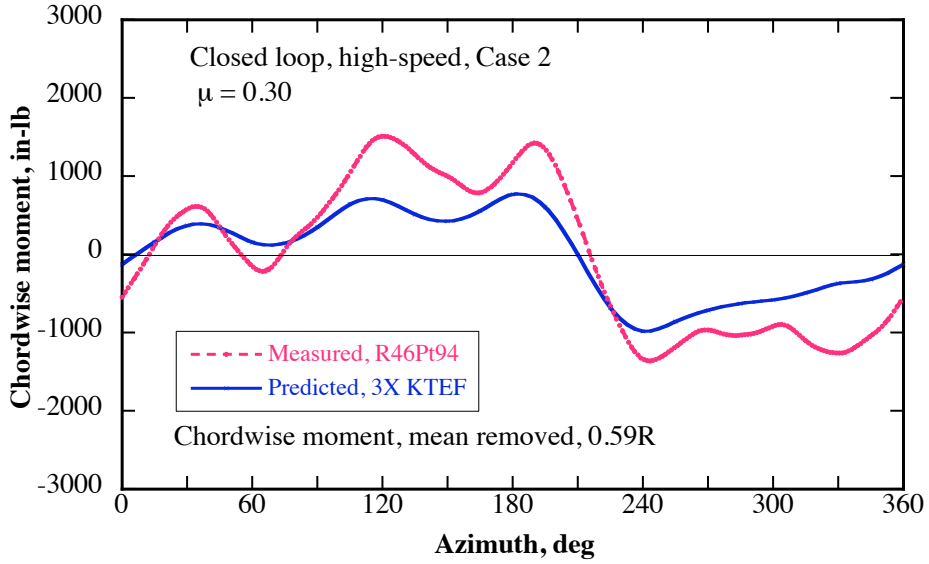

Fig. 4g. Chordwise moment correlation, 0.59R, closed loop Case 2

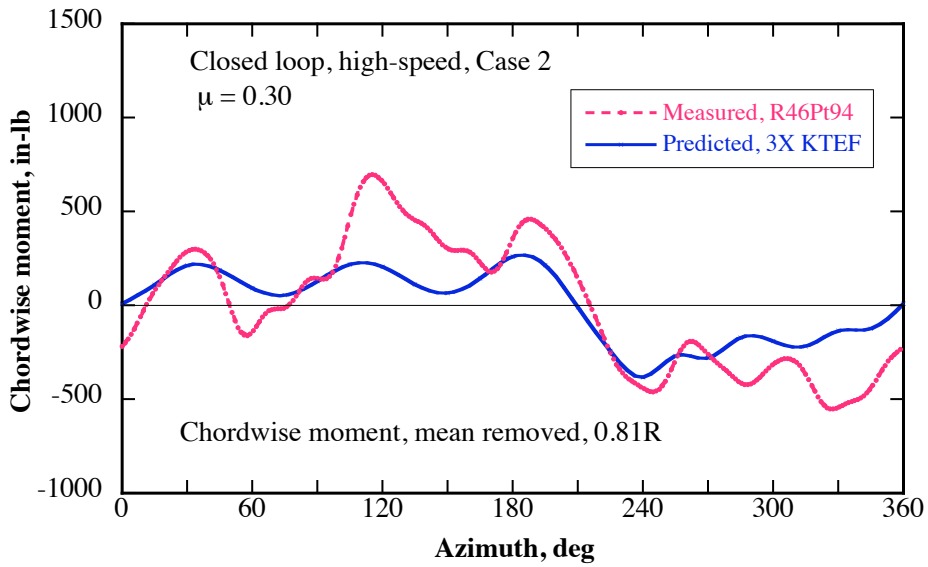

Fig. 4h. Chordwise moment correlation, 0.59R, closed loop Case 2.

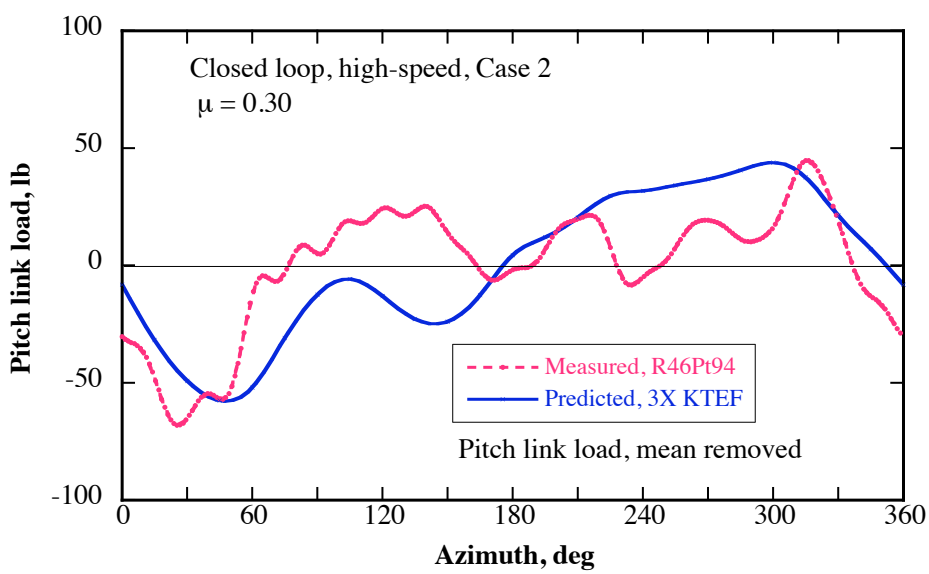

Fig. 4i. Pitch link load correlation, closed loop, Case 2.

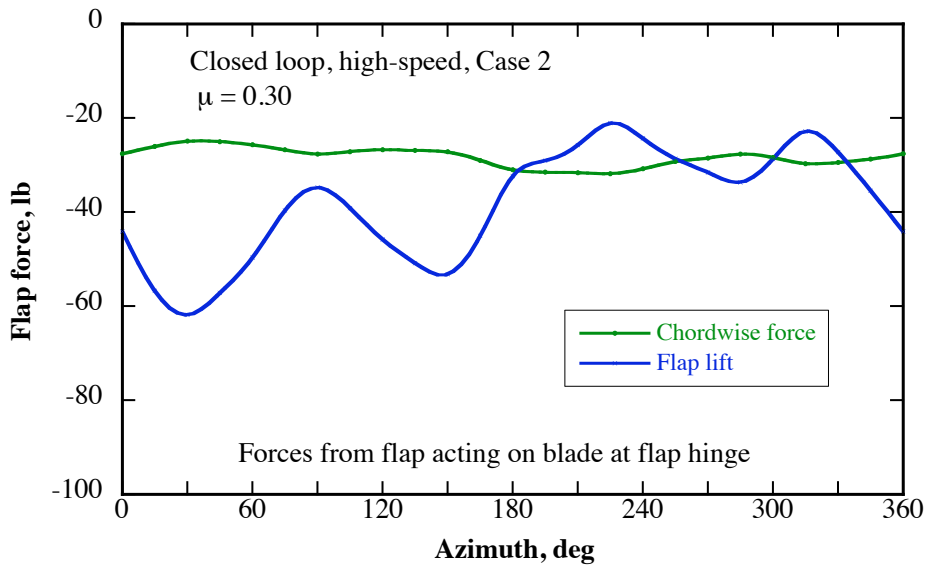

Fig. 4j. Predicted flap forces, closed loop Case 2.

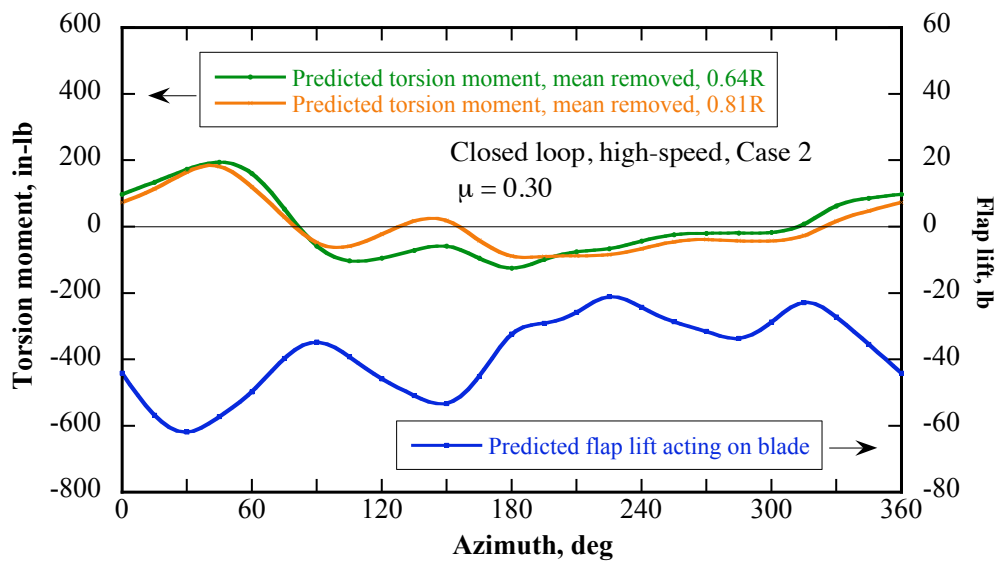

Fig. 4k. Predicted effect of flap on blade, closed loop Case 2.

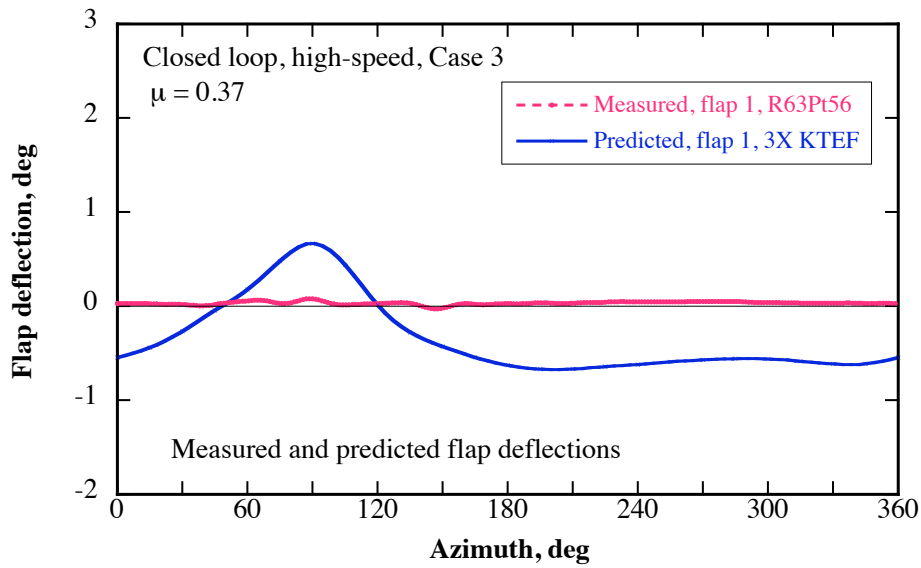

Fig. 5a. Measured and predicted flap deflections, closed loop Case 3.

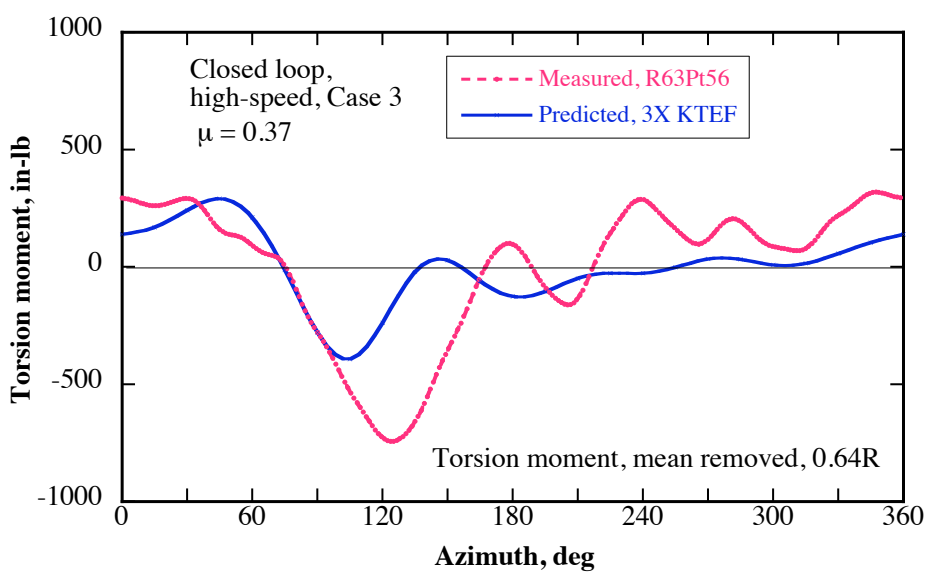

Fig. 5b. Torsion moment correlation, 0.64R, closed loop Case 3.

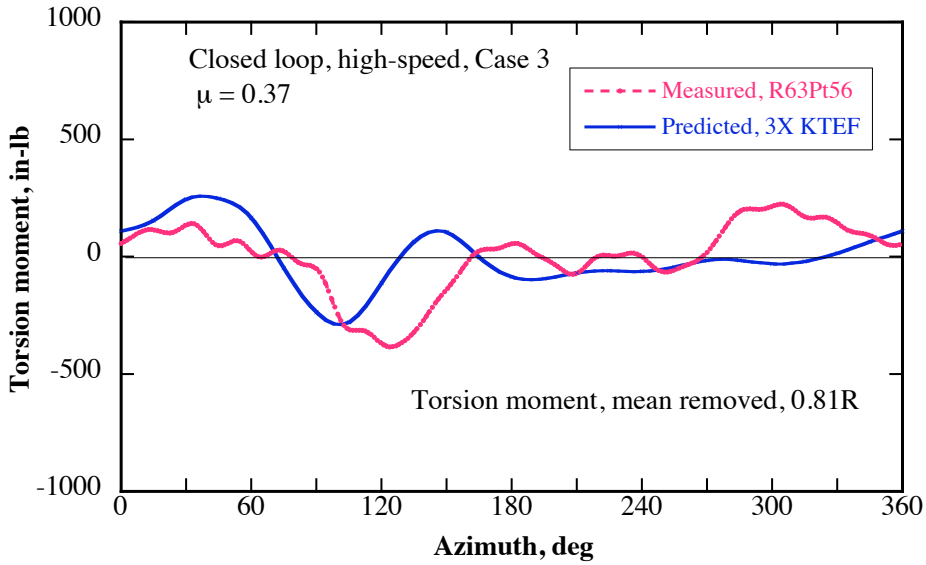

Fig. 5c. Torsion moment correlation, 0.81R, closed loop Case 3

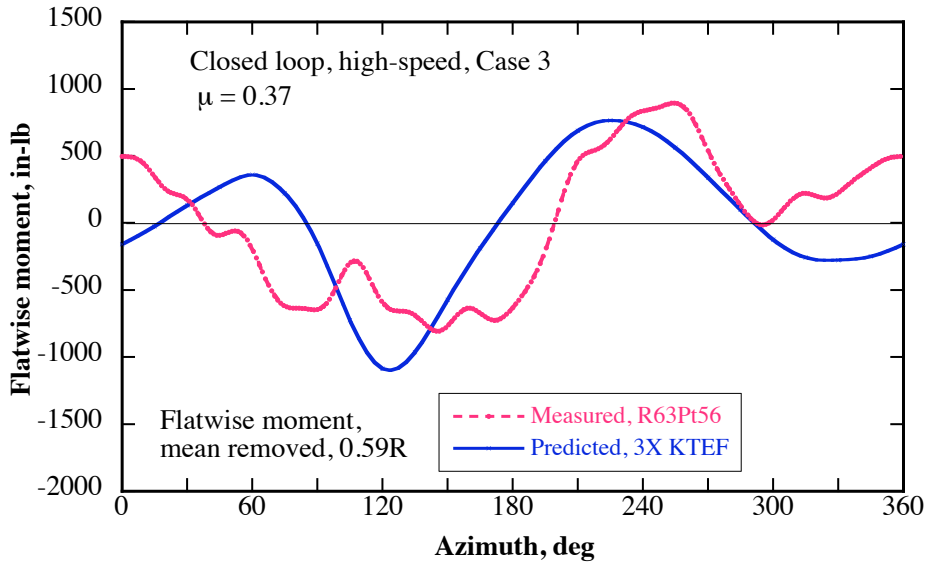

Fig. 5d. Flatwise moment correlation, 0.59R, closed loop Case 3

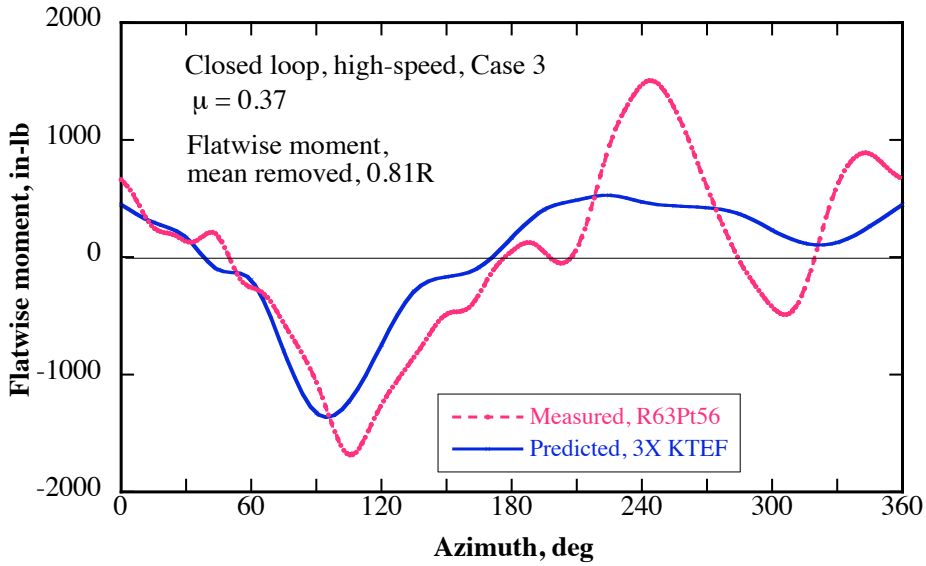

Fig. 5e. Flatwise moment correlation, 0.81R, closed loop Case 3

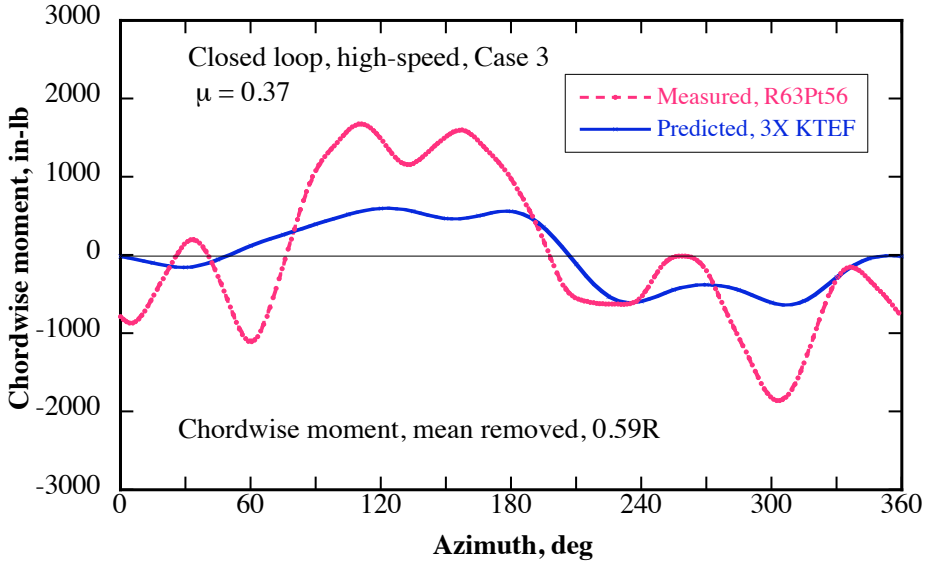

Fig. 5f. Chordwise moment correlation, 0.59R, closed loop Case 3

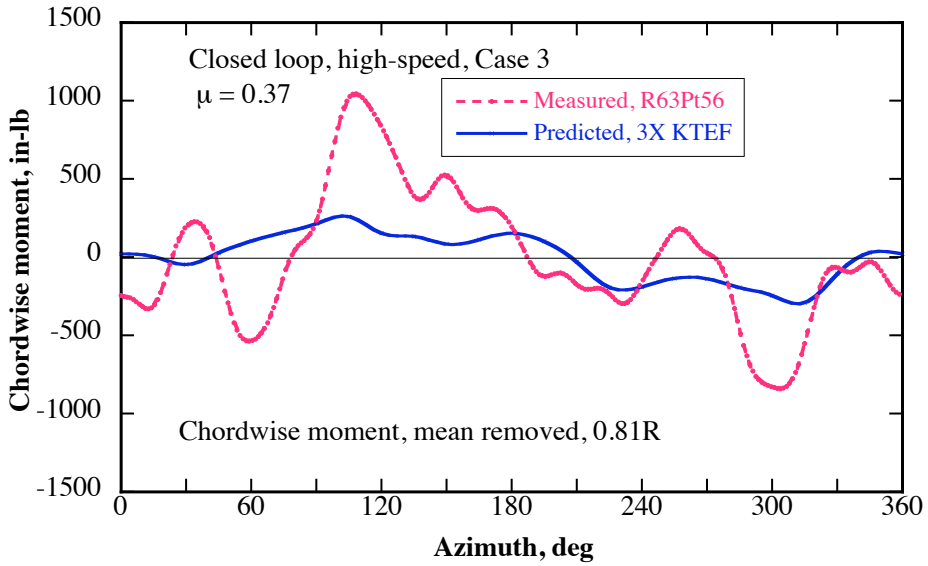

Fig. 5g. Chordwise moment correlation, 0.81R, closed loop Case 3

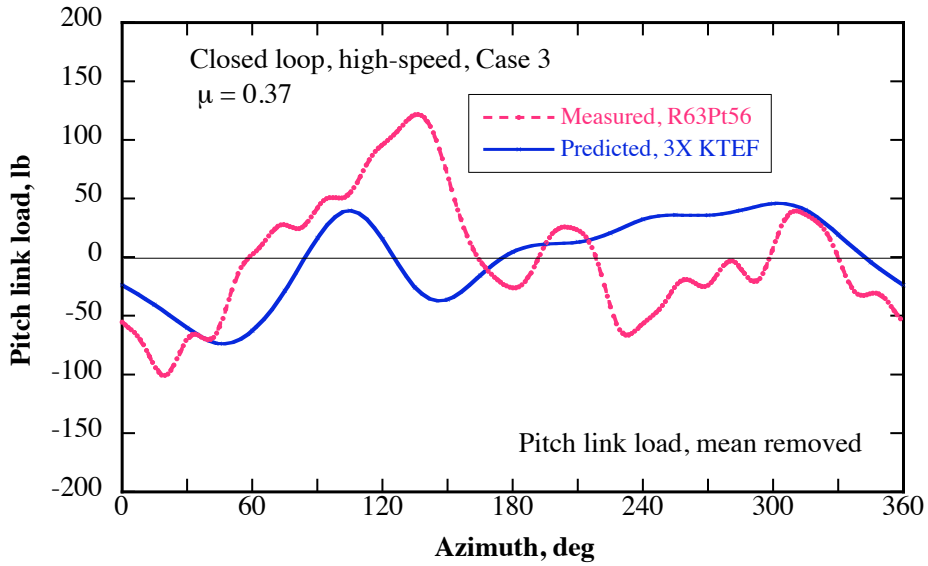

Fig. 5h. Pitch link load correlation, closed loop Case 3.

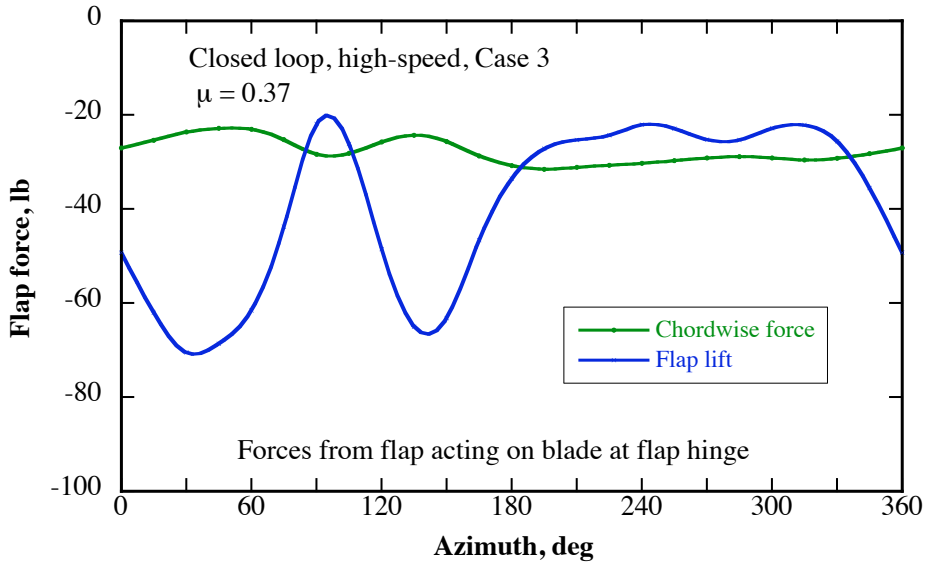

Fig. 5i. Predicted flap forces, closed loop Case 3

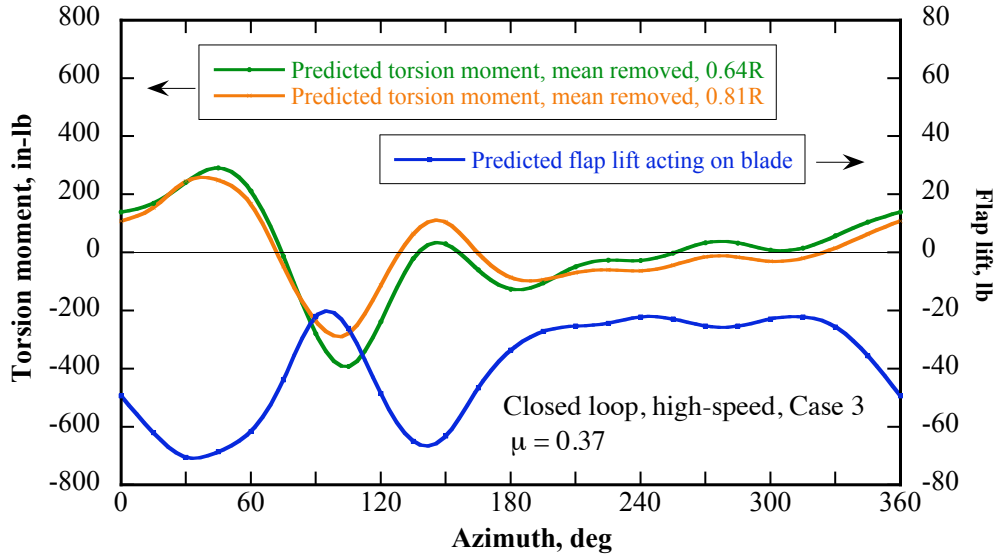

Fig. 5j. Predicted effect of flap on blade, closed loop Case 3.

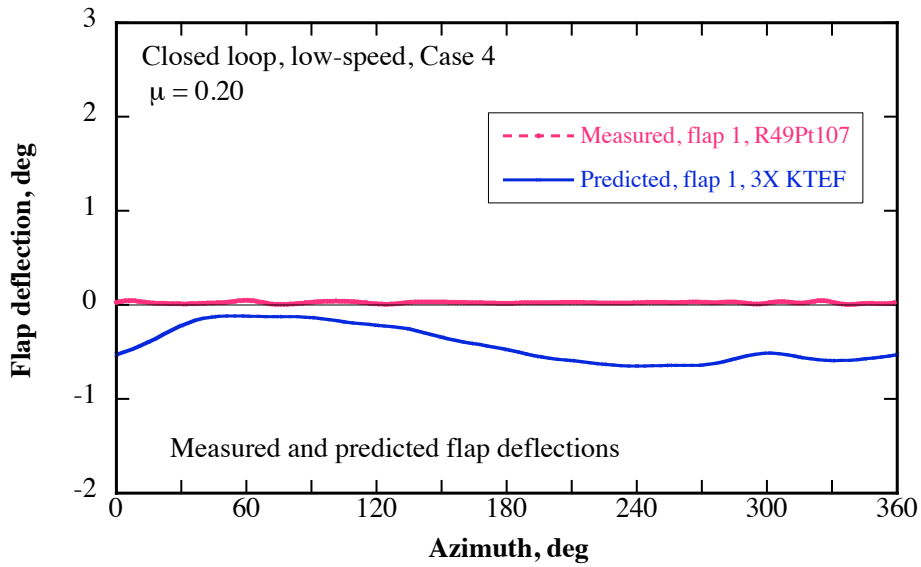

Fig. 6a. Measured and predicted flap deflections, closed loop Case 4.

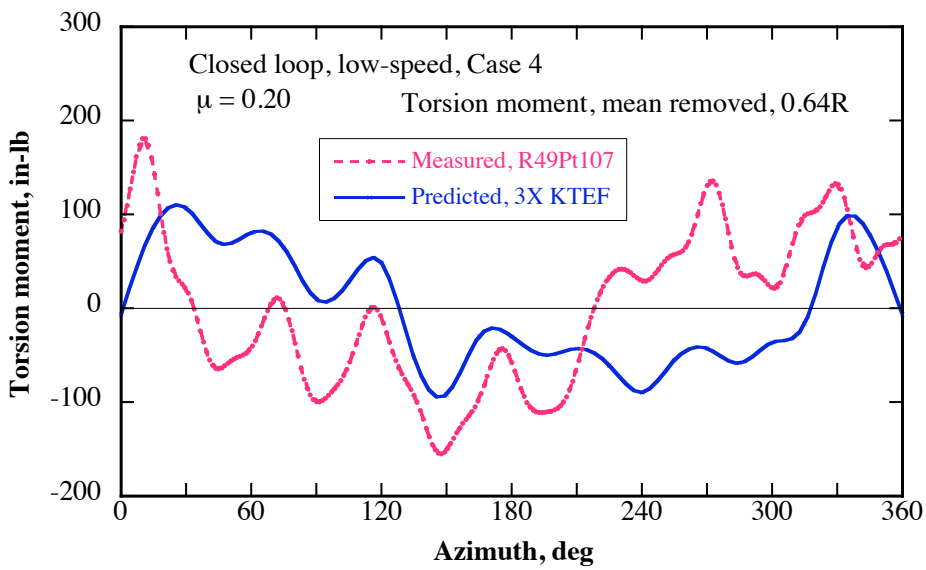

Fig. 6b. Torsion moment correlation, 0.64R, closed loop Case 4.

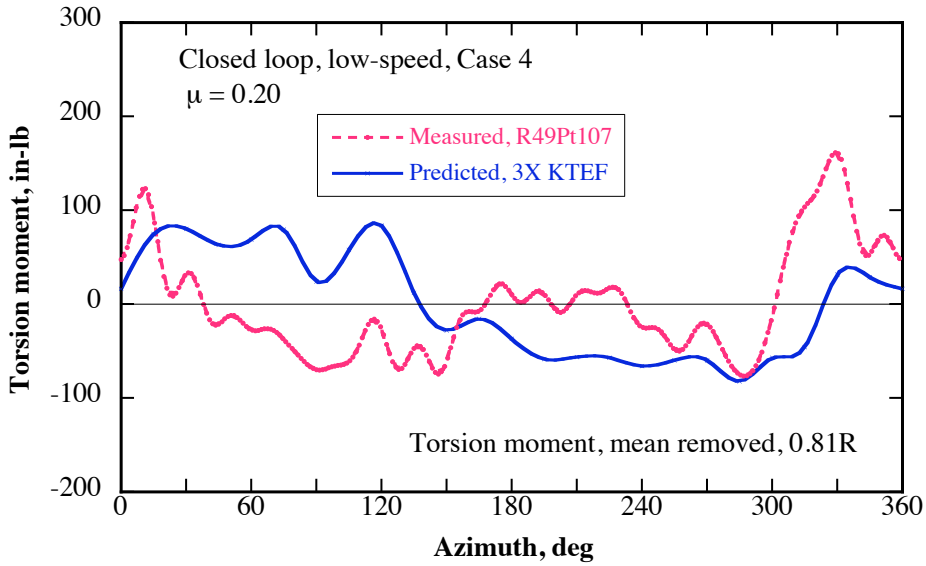

Fig. 6c. Torsion moment correlation, 0.81R, closed loop Case 4.

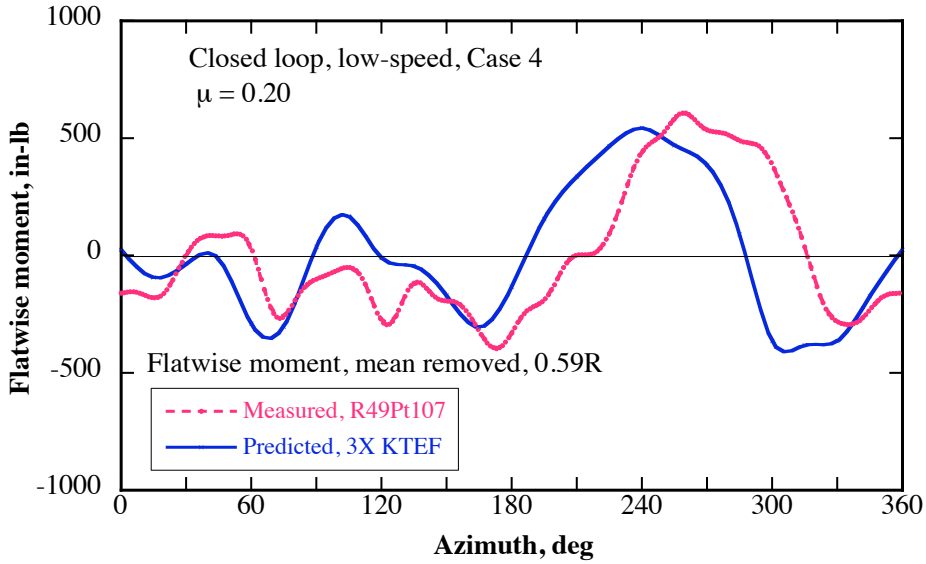

Fig. 6d. Flatwise moment correlation, 0.59R, closed loop Case 4.

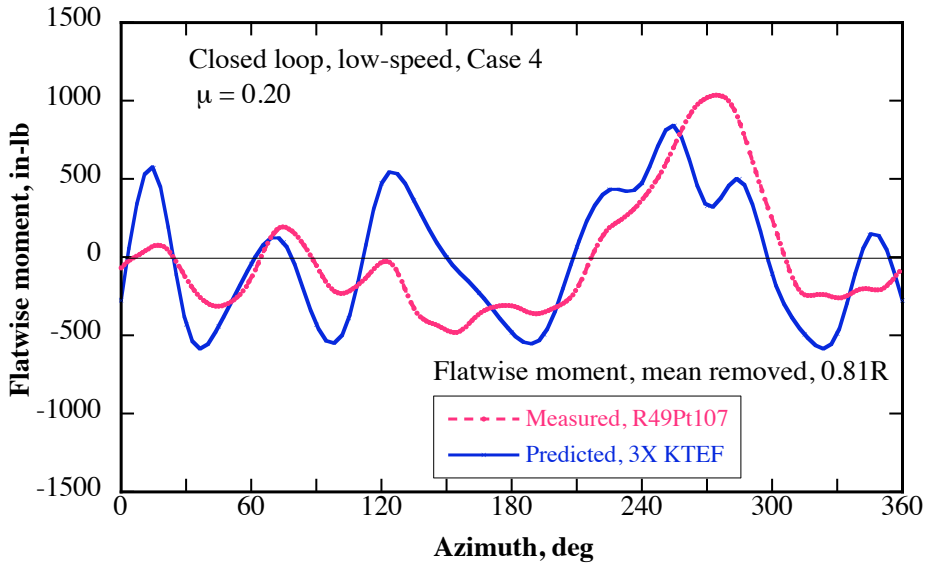

Fig. 6e. Flatwise moment correlation, 0.81R, closed loop Case 4.

.

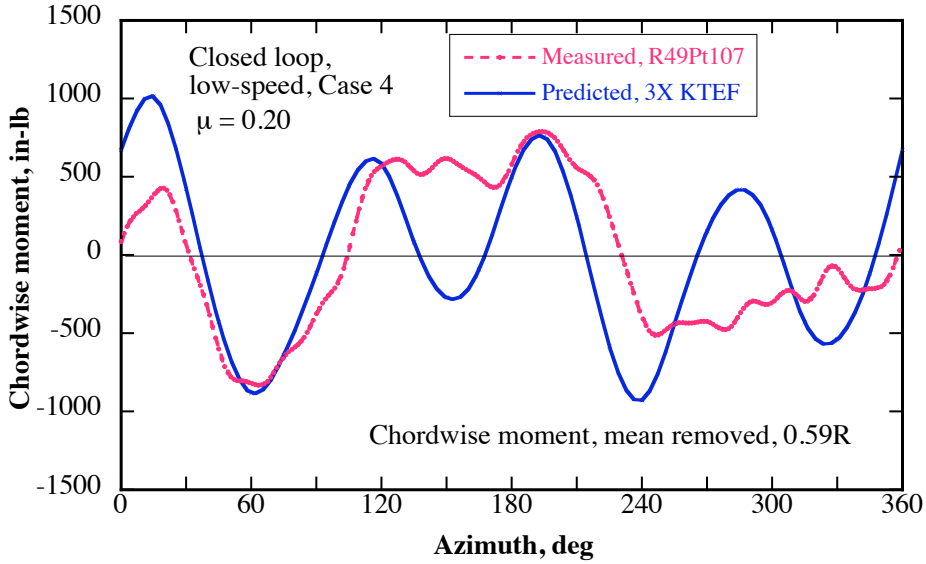

Fig. 6f. Chordwise moment correlation, 0.59R, closed loop Case 4.

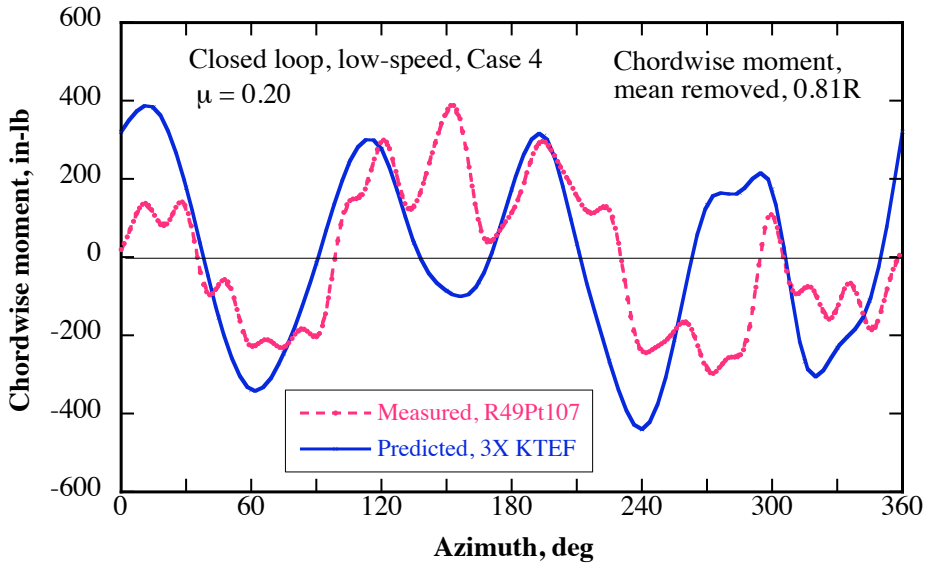

Fig. 6g. Chordwise moment correlation, 0.81R, closed loop Case 4.

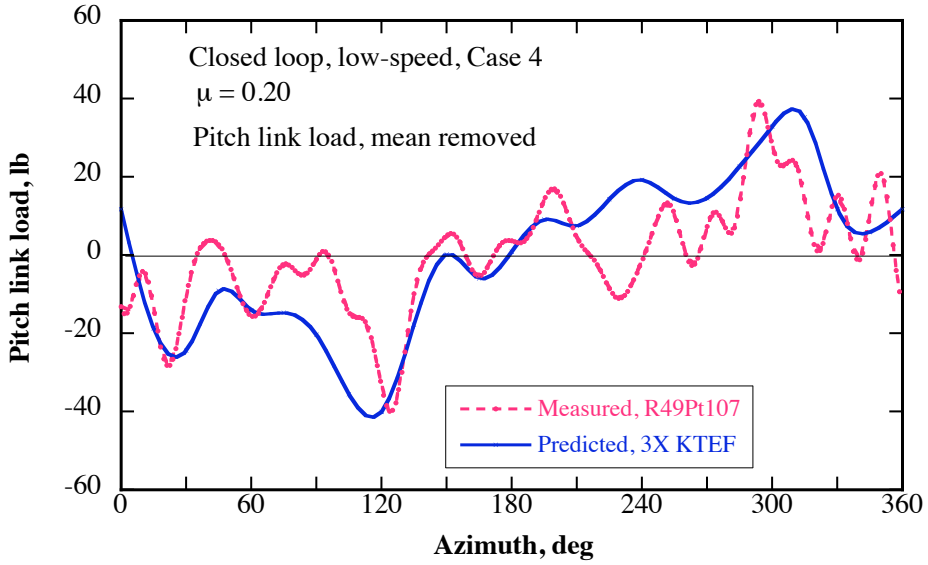

Fig. 6h. Pitch link load correlation, closed loop Case 4.

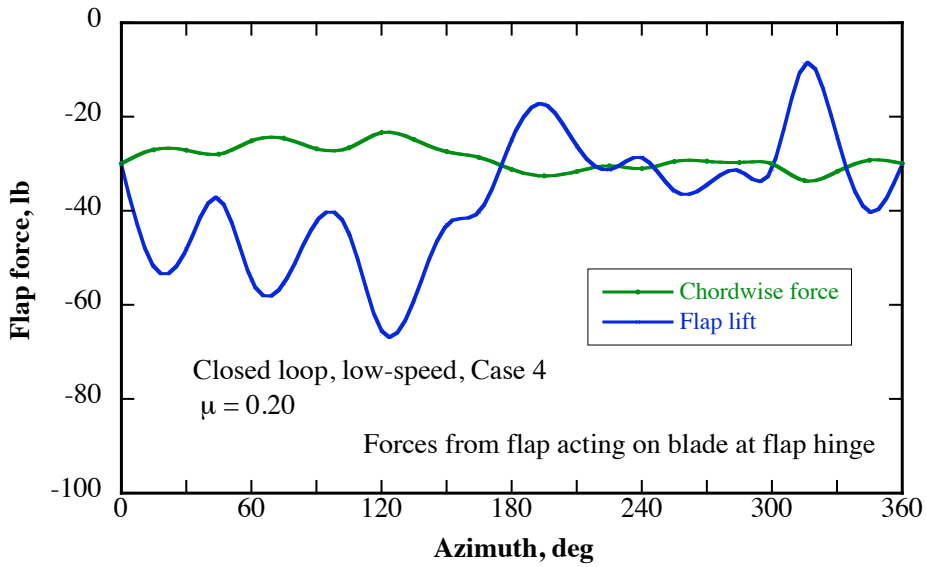

Fig. 6i. Predicted flap forces, closed loop Case 4.

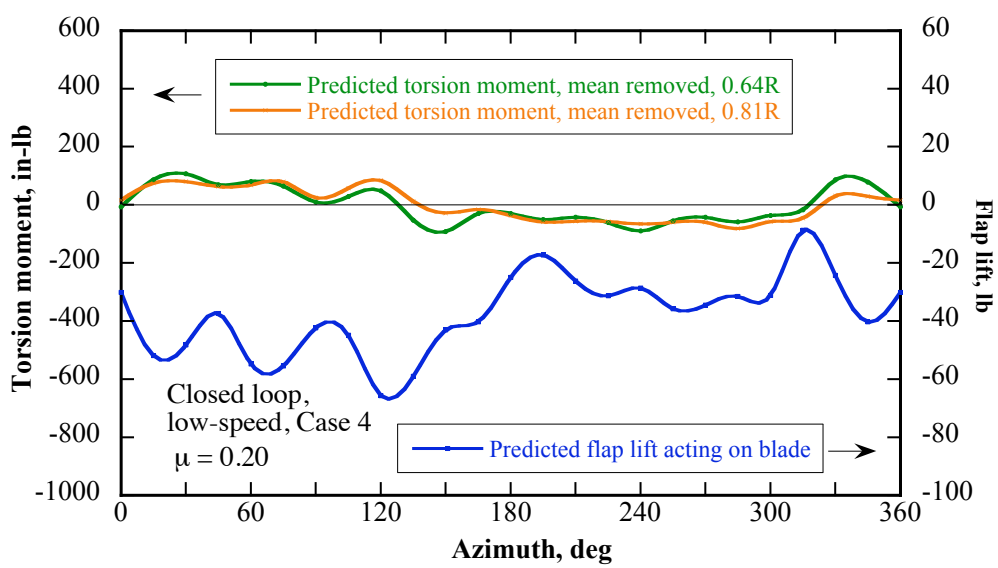

Fig. 6j. Predicted effect of flap on blade, closed loop Case 4.

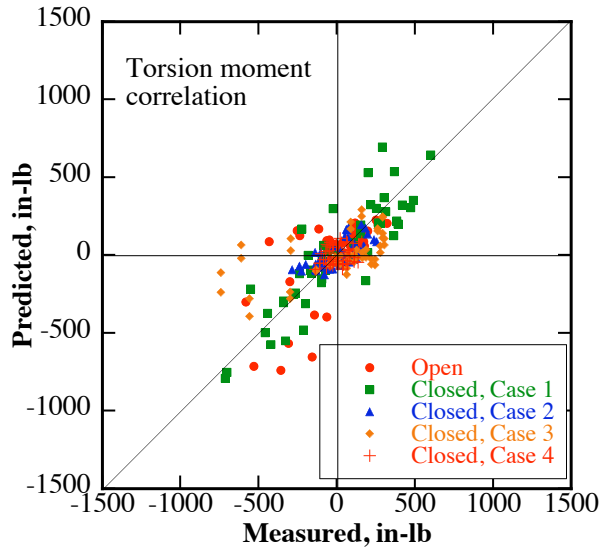

Fig. 7a. Torsion moment correlation.

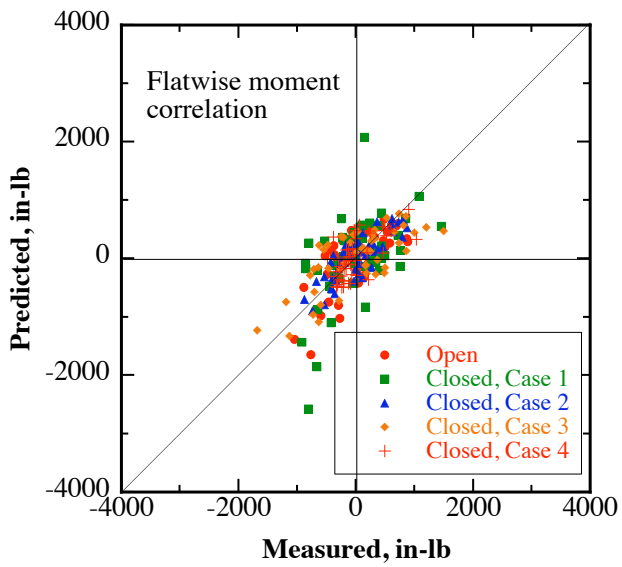

Fig. 7b. Flatwise moment correlation.

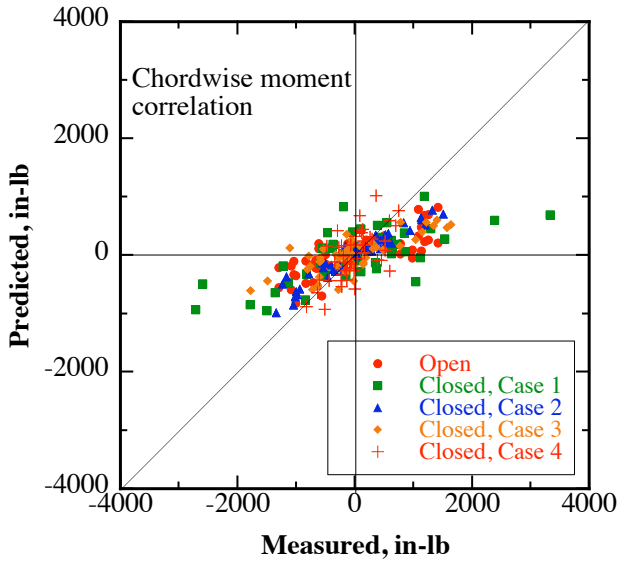

Fig. 7c. Chordwise moment correlation.

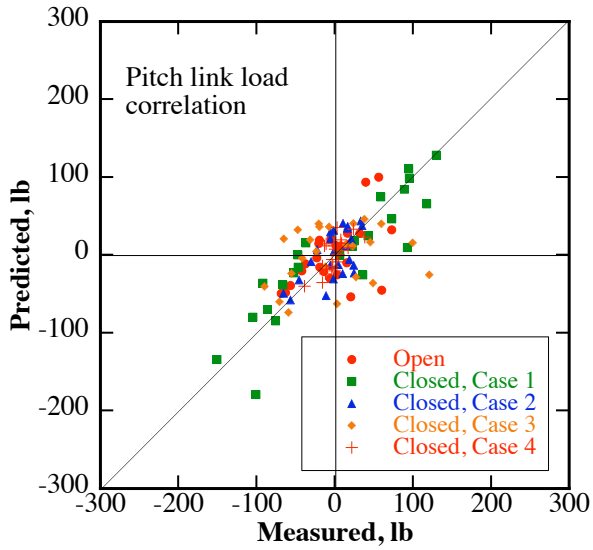

Fig. 7d. Pitch link load correlation.